

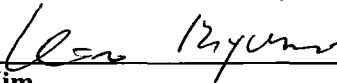
Dual-LED Bio-agent Detection System Design Based on FPGA


BY

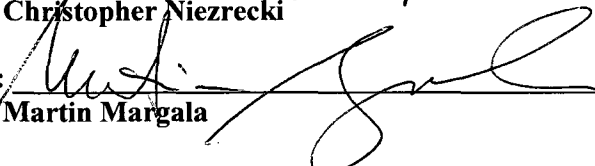
YUNFENG LING

SUBMITTED IN PARTIAL FULFILLMENT OF THE REQUIREMENTS
FOR THE DEGREE OF MASTER OF SCIENCE
DEPARTMENT OF MECHANICAL ENGINEERING
UNIVERSITY OF MASSACHUSETTS LOWELL
2010

Signature of Author:  Date: Apr. 16. 2010.

Signature of Thesis Supervisor: 
Byungki Kim

Signatures of Other Thesis Committee Members:
Committee Member Signature: 
Christopher Niezrecki

Committee Member Signature: 
Martin Margala

UMI Number: 1485448

All rights reserved

INFORMATION TO ALL USERS

The quality of this reproduction is dependent upon the quality of the copy submitted.

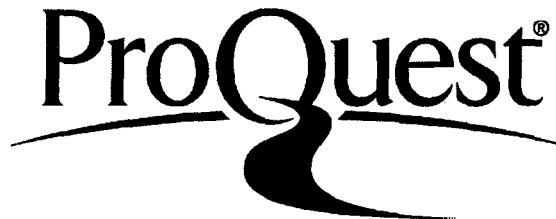
In the unlikely event that the author did not send a complete manuscript and there are missing pages, these will be noted. Also, if material had to be removed, a note will indicate the deletion.



UMI 1485448

Copyright 2010 by ProQuest LLC.

All rights reserved. This edition of the work is protected against unauthorized copying under Title 17, United States Code.



ProQuest LLC
789 East Eisenhower Parkway
P.O. Box 1346
Ann Arbor, MI 48106-1346

Dual-LED Bio-agent Detection System Design Based on FPGA

BY

YUNFENG LING

**ABSTRACT OF A THESIS SUBMITTED TO THE FACULTY OF THE
DEPARTMENT OF MECHANICAL ENGINEERING
IN PARTIAL FULFILLMENT OF THE REQUIREMENTS
FOR THE DEGREE OF
MASTER OF SCIENCE
UNIVERSITY OF MASSACHUSETTS LOWELL
2010**

Thesis Supervisor: Byungki Kim, Ph.D.

Assistant Professor, Department of Mechanical Engineering

ABSTRACT

Label-free optical biosensors have a wide range of applications from biomedical research to bio-defense monitoring of known or potential bioterrorist threats. But currently, there are few commercial real-time portable bio-agent detection devices available. In this thesis a potential of bio-agent detection method, reflectometric interference spectroscopy (RIfS), for a compact label-free biosensor was investigated. A model to estimate sensitive layer thickness variation on the sensor chip was developed.

The prototype using Altera Cyclone III FPGA chip as the main processor core was built in the design. The bio-agent detection device consists of four main parts, which include a dual-LED sensor module, a Field-Programmable Gate Array (FPGA) board, an interface circuit board, and a power supplier. The LEDs' signal is converted into digital data by interface board and processed by the FPGA board. The measurement results are shown by the interface board. The device is powered by a nine-volt battery (PP3 battery), which enables portability of the device. Meanwhile, the wireless communication module is integrated into the bio-agent detection system to operate as a network sensor.

To verify the model and FPGA sensor device, two experiments with different samples were carried out. The estimated values by dual-LED sensor were

compared with the reference values, which were measured by the spectrum shift method. The results indicate that the thickness variations measured by the dual-LED sensor agree with the reference values well within the range from 2 to 15 nm.

Thus, the contribution of the thesis is developing a model to estimate sample layer thickness variation and its validation using the dual-LED detection system based on FPGA. The design and fabrication of the system is also main contribution in this thesis.

Keywords: Biosensor, Film Thickness Variation Measurement, Reflectometric Interference Spectroscopy (RIfS), Field-Programmable Gate Array (FPGA), Light Emitting Diode (LED)

ACKNOWLEDGEMENTS

I am deeply indebted to my supervisor Prof. Byungki Kim from the Department of Mechanical Engineering, and thank his guidance, support throughout this work and his continued encouragement during the research and writing of this thesis.

I want to thank Prof. Christopher Niezrecki from Department of Mechanical Engineering and Martin Margala from the Department of Electrical & Computer Engineering, the members of the thesis committee, for their helpful discussions and suggestions.

I would like to express my gratitude to Prof. Melisenda J. McDonald, Prof. Xingwei Wang, Prof. Martin Margala, and Dr. Wenhui Wang, who helped and supported me during this time and give me the possibility to complete this thesis. Also, Sai Rahul Chalamalasetti, Nan Wu, and Leslie Farris, as my project partners, deserve recognition for their hard work and help in this research work.

Finally, I give thanks to my parents, Wenxian Fan and Yongchang Ling, and my friends for their support throughout this research.

TABLE OF CONTENTS

ABSTRACT.....	ii
ACKNOWLEDGEMENTS.....	iv
LIST OF TABLES.....	vii
LIST OF FIGURES	viii
GLOSSARY OF TERMS	xi
Chapter 1 Introduction.....	1
1.1 Overview.....	3
Chapter 2 Modeling of Thickness Variation	5
2.1 Planar optical sensor based on reflectometric interference spectroscopy.....	5
2.2 Discrete wavelength determination.....	7
2.3 Modeling for film thickness variation.....	8
2.3.1 Spectrum Shift Method.....	9
2.3.2 Dual-LED method.....	10
Chapter 3 System Design	13
3.1 Dual-LED Sensor.....	14
3.2 Interface Circuit Board	17
3.3 FPGA board and DHL Program Design.....	22
3.3.1 System Synchronizer	23
3.3.2 Sensor LED Controller	25
3.3.3 ADC Control Module	26
3.3.4 Data Processing Module	28
3.3.5 Results Display Module.....	29
3.3.6 Wireless Communication Module	30
3.4 Casing design and fabrication.....	33

3.5	External wireless communication Module.....	34
3.6	Application design for Work PC.....	35
Chapter 4	Results and Discussion	37
4.1	Experiments	37
4.1.1	Experiments with sample chips with step difference.....	38
4.1.2	Experiments with Protein G' binding	42
4.2	Discussion	45
Chapter 5	Conclusions.....	46
	RECOMMENDATIONS.....	48
	APPENDIX A.....	49
	AUTHOR BIOGRAPHY.....	58

LIST OF TABLES

	Page
Table 3.1 Signal definition of system synchronizer	24
Table 3.2 Signal definition of sensor LED control module	26
Table 3.3 Signal definition of the ADC interface	27
Table 3.4 Signal definition of the data processing module	29
Table 3.5 Signal definition of the results display module.....	30
Table 3.6 Signal definition of the wireless communication module.....	31
Table 4.1 Measurement results of the thickness variation for the first experiments.....	41
Table 4.2 Measurement results of thickness variation for the second experiments.....	44
Table A.1 Pin assignment of the system	51

LIST OF FIGURES

	Page
Figure 2.1 Schematic diagram of planer optical biosensor.....	6
Figure 2.2 Schematic diagram of the two wavelength spectrum shift monitoring	7
Figure 2.3 Simulated spectrum shift in the interference pattern.....	9
Figure 3.1 Diagram of the dual-LED bio-agent detection system device based on FPGA	13
Figure 3.2 Diagram of the wireless dual-LED bio-agent detection system.....	14
Figure 3.3 Schematic diagram of the measurement system.....	15
Figure 3.4 Schematic of the dual-LED sensor.....	15
Figure 3.5 Spectral responsivity of the photo detector	16
Figure 3.6 Diagram of the interface board	17
Figure 3.7 Schematic of the operation interface.....	18
Figure 3.8 Schematic of the sensor control circuit.....	18
Figure 3.9 Schematic of the data acquisition module.....	19
Figure 3.10 Schematic of the module	20
Figure 3.11 Schematic of the communication interface	21
Figure 3.12 Schematic of the power supply.....	21
Figure 3.13 CMCS002 module FPGA board.....	22
Figure 3.14 Diagram of system synchronizer	23

Figure 3.15 Diagram of the sensor LED control module.....	25
Figure 3.16 Block diagram of the ADC interface.....	28
Figure 3.17 Diagram of the data processing module	28
Figure 3.18 Diagram of the results display module.....	30
Figure 3.19 Diagram of the wireless communication module.....	31
Figure 3.20 Data packet format	32
Figure 3.21 Picture of the casing	34
Figure 3.22 PC Application for data receiving and processing	35
Figure 4.1 Pictures of the system prototype.....	37
Figure 4.2 Picture of the sensor holder part.....	38
Figure 4.3 Sample diagram	39
Figure 4.4 Spectrum and spectrum shift of different sample chips	39
Figure 4.5 Normalized spectrum profile and simulated spectrum by second order polynomials.....	40
Figure 4.6 Intensity variation along the sample three chip.....	41
Figure 4.7 Thickness variation measured by the dual LEDs sensor and spectrum shift method	41
Figure 4.8 Spectrum of the sample with a PMMA layer	42
Figure 4.9 Spectrum profile and simulated spectrum by second order polynomials for biochips with a PMMA layer	43
Figure 4.10 Spectrum of sample three	44

Figure 4.11 Thickness variation measured by the dual LEDs sensor and spectrum shift method	44
Figure A.1 Schematic of interface circuit board	49
Figure A.2 Diagram of the RTL structure of FPGA board.....	50

GLOSSARY OF TERMS

Acronym

FPGA	Field-Programmable Gate Array
HDL	Hardware Description Language
RTL	Register Level
LED	Light-emitting Diode
ADC	Analog to Digital Converter
PMMA	Poly (methyl methacrylate)
RIIS	Reflectometric Interference Spectroscopy

Chapter 1 Introduction

A biosensor is a device that is used to detect an analyte that combines a biological component with a physicochemical detector component. [1] Biosensors have been applied to detect various biomolecular complexes in many kinds of fields such as public health security, food industry and drug monitoring. [2, 3]

In typical biosensors, detection of specific pathogens or proteins begins with immobilizing appropriate bioreceptors on the sensing areas of a chip. When analytes are introduced into those areas, only the target biomolecules will be bound to their corresponding biomolecular receptors. This binding process is usually monitored with commercial analytical technique that requires transduction labeling elements, such as fluorescent dyes or radioactive isotopes, to generate a physically readable signal from a recognition event. [4, 5] But the disadvantage is that labeling chemistry is expensive and time-consuming. In contrast, recent progress in label-free biosensing systems, in which biomolecules are unlabeled or unmodified, has shown promising results.

Label-free biosensors are devices that use biological or chemical receptors to detect analytes (molecules) in a sample. [6] The detailed information on the selectivity and affinity can be acquired by these sensors. In many cases, the binding kinetics and thermodynamics of an interaction can be detected. [7] Due to its accuracy and stability, the optical label-free sensors are investigated extensively among different applications. The sensing transduction signals in optical label-free biosensing platforms are based on small changes in refractive index caused by the immobilization or binding reaction of

biomolecules. Many biomolecular binding interactions are measured by the photonic structures of these photonic sensing biochips, including surface plasmon resonance [8, 9], interferometers [10-13], resonators [14, 15], gratings [16, 17], and photonic crystals [18, 19].

In this thesis, the optical label-free sensor based on interferometers was adopted. [20, 21] The sensitivity in the detection of Influenza A Nucleoprotein through the combination of the PMMA based orientation method and label-free interferometric detection based on RIIS has been increased by the studies. [22-24] Although this method employed in the research is highly sensitive and stable, variation in thickness of the sensitive layer on the sensor chip surface has yet to be examined. In this thesis, the model of the sensitive layer thickness variation was proposed.

Typically, a large and expensive spectrometer, which includes a tunable laser or a wide band light source and an optical spectrum analyzer, has been used in the experiments. [25] The potential of this kind of sensor is limited because of expensive and bulky components, which make the devices less cost effective. With the advances in electronics and optics, especially LED techniques, compact devices have become feasible. In this design, by using dual light-emitting diodes (LED) and a photo detector with a FPGA circuit board, the handheld device for bio-agent detection may become practical. The bio-agent detection device consists of four main parts, which include a dual-LED sensor module, a Field-Programmable Gate Array (FPGA) board, an interface circuit board, and a power supplier. The dual-LED sensor is used to detect the bio-agent in the atmosphere. The LEDs' signal is converted into digital data by interface board and processed by the FPGA board. The measurement results are shown by the interface board.

The device is advantageous because it can operate in real-time without the difficult labeling step required for detection with many bioanalytical techniques. The prototype using the Altera Cyclone III FPGA chip as main processor core is fabricated in the project. The device is powered by a nine-volt battery (PP3 battery), which enables portability of the device.

Two types of experiments with different kinds of samples were carried out to verify the model and the FPGA sensor device. In the first experiment, the samples sensor chips with different oxidized silicon layer thickness at both sides were used. The thickness difference on one sensor chip simulated sensitive layer changes on the real sensor chip introduced by the bio-reaction binding. With these samples, the model and device can be tested with a larger range of the thickness variation. In the second experiment, the dual-LED sensor coupled with a functional Poly(methyl methacrylate) (PMMA) thin film coated onto an oxidized silicon wafer was tested. The thickness variations caused by recombinant Protein G' binding to the PMMA layer with different incubation time were measured. The results by the spectrum shift method and the dual-LED method were compared.

1.1 Overview

In chapter #2, a generalized procedure to model the thickness variation of sensitive layer on the sensor chip is presented. Firstly, the variation is measured by the spectrum shift method. Then the dual-LED method is proposed as well. In chapter #3, the bio-agent detection device based on FPGA is proposed. The structure and functions of the main parts of the system are introduced. In chapter #4, two types of different experiments

are designed to verify the model proposed in chapter #2. The prototype of sensor system is tested in this chapter. The measurement results by different methods are presented and are compared. In chapter #5, the conclusions of this work are made. Recommendations for future work are presented as well.

Chapter 2 Modeling of Thickness Variation

This section focuses on the principle of the Reflectometric interference spectroscopy (RIfS) planer optical label-free bio-agent detection and modeling. The model of the thickness change of the sensitive layer on the sensor chip is derived by different approaches. In the first method, the spectrometer is employed to build the model. In order to reduce the cost and size of the setup, the dual-LED sensor is investigated and the model based on the dual-LED sensor is proposed as the second method.

2.1 Planar Optical Sensor Based on Reflectometric Interference Spectroscopy

RIfS is a physical method based on the interference of light beam at thin films, which is used as a detection method in chemo- and biosensors. [32-34]

As seen in Figure 2.1, the light is directed onto a multiple-layer system on a biosensor chip. One part of the light is reflected at the top surface of the thin layer, and the other penetrates the layer, and then is reflected at the other interface. These two partial reflected beams superimpose and form an interference pattern, resulting in constructive or destructive interference depending on the angle of incidence, wavelength, and optical density of the layers, which is given by optical thickness of the layer, defined by the product of refractive index and physical thickness of the layer. On the top surface of the sensor chip, an additional layer is chemically modified, used to interact with target molecules, resulting in a change in the optical thickness of the layer. An optical thickness change gives rise to a modulation of the interference spectrum. The molecular interaction

can be investigated by observation of the binding behavior of the target molecules, through monitoring the change in optical thickness over times. This simplified version of ellipsometry, called reflectometric interference spectroscopy, provides a simple and robust technique in chemosensing and biosensing. [35]

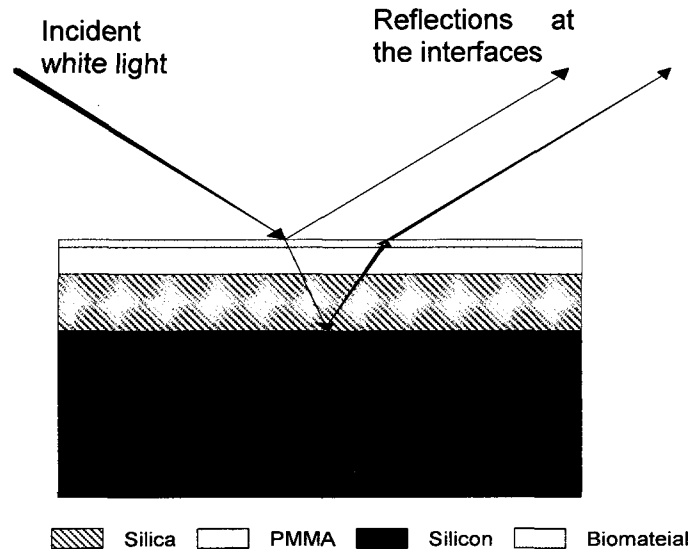


Figure 2.1. Schematic diagram of planer optical biosensor

In this thesis, PMMA serves as the functional biomaterial binding layer. [36] The effective thickness of the PMMA layer will increase slightly when the biomaterial binds on the surface of PMMA. Therefore, the optical path length or the Fabry Perot (FP) cavity length changes as shown in Figure 2.1. This variation causes shift of the reflection spectrum as shown in Figure 2.2. By monitoring the spectrum shift, we can determine whether there is a significant bound biomaterial on the surface. [37]

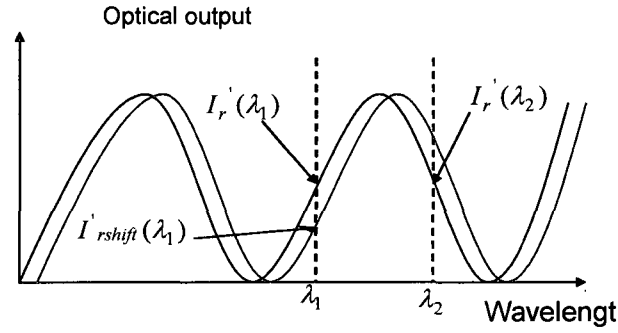


Figure 2.2. Schematic diagram of the two wavelength spectrum shift monitoring

2.2 Discrete Wavelength Determination

A small shift, caused by the sensitive layer thickness variation, can be distinguished by monitoring the reflectometric interference spectrum. A spectrometer with a wide band light source, usually a tungsten halogen lamp, is used in the measurement. The spectrometer is usually expensive and has a large size, so it's not suitable for compact applications. With a high power consumption in the spectrometer, heat problems can be a big issue in the application. With the advance in electronics and optics, especially LED techniques, compact light sources have become feasible. In this design, the spectrometer is replaced by dual LEDs to measure the spectrum shift at discrete wavelengths. Two wavelengths at the each slope of a peak or trough are used. When the spectrum shift from left to right, one output will increase, the other will decrease, so their difference will increase. However, because of the interference from the atmosphere, the spectrum also moves up or down. Outputs of the detector at these two wavelengths increase or decrease simultaneously, but their difference does not change. The intensity difference between two LEDs is only related to left or right spectrum shift, even if spectrum moves up or down and left or right. Therefore, the determination of

error from the interference can be reduced by this method. Meanwhile, the size and power consumption of the sensor are reduced using two LEDs and one photo detector.

2.3 Modeling of Thickness Variation

The reflected beams I_{r1} and I_{r2} are superposed at the front side of the sensitive layer on the sensor as shown in Figure 2.1. This superposition produces an interference pattern, which is dependent on the optical thickness of the transparent layer between the two interfaces. The intensity of total reflected intensity I_r can be calculated by, [38]

$$I_r(\lambda) = I_{r1} + I_{r2} + 2\sqrt{I_{r1}I_{r2}} \cos\left(\frac{2\pi}{\lambda}(\Delta_l + \delta_l)\right) \quad (2.1)$$

where I_{r1} and I_{r2} are the intensity of the reflected beam at the front and back sides of the sensitive layer of the sensor. Δ_l is the optical path difference caused by the thin film layer. δ_l is the path length difference variation introduced by the affinity on the sensitive layer. The optical path difference between two reflected light beams is derived as,

$$\Delta_l = 2d\sqrt{(n^2 - \sin^2 \theta)} \quad (2.2)$$

where d is the physical thickness of the sensitive layer. n is the refractive index of the layer. θ is the angle of the incident beam in reference to the perpendicular. The variation of the optical path difference is expressed as,

$$\delta_l = 2\Delta d\sqrt{(n^2 - \sin^2 \theta)} \quad (2.3)$$

where Δd is the variation of the physical thickness of the sensitive layer.

Due to this physical thickness change, the optical path difference increases, resulting into a spectrum shift in the interference pattern, as shown in Figure 2.3. This

shift is measured to calculate the physical thickness change.

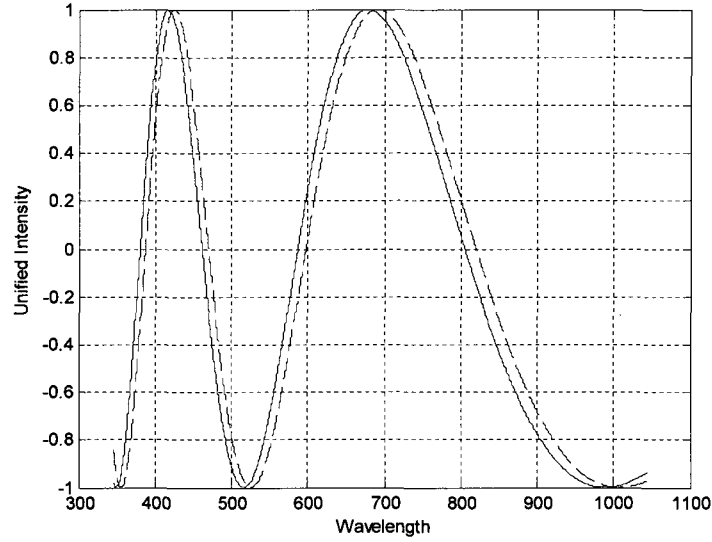


Figure 2.3. Simulated spectrum shift in the interference pattern

2.3.1 Spectrum Shift Method

From equation (2.1), at a specific wavelength, the phase of the reflected light beam has the same phase as the one with a spectrum shift after a thickness change.

$$\Phi = \frac{2\pi\Delta_l}{\lambda_s} = \frac{2\pi(\Delta_l + \delta_l)}{\lambda_s + \Delta_\lambda} \quad (2.4)$$

where λ_s is the wavelength at which the spectrum shift is measured, and Δ_λ is the spectrum shift. Then the relationship between spectrum shift and optical path difference variation is derived as,

$$\frac{\Delta_\lambda}{\lambda_s} = \frac{\delta_l}{\Delta_l} \quad (2.5)$$

Then we can get optical path difference variation,

$$\delta_l = \frac{\Delta_\lambda}{\lambda_s} \cdot \Delta_l \quad (2.6)$$

The optical path difference can be calculated from the spectrum data as follow,

$$\Phi_{diff} = \frac{2\pi}{\lambda_{max2}} \Delta_l - \frac{2\pi}{\lambda_{max1}} \Delta_l = 2\pi \quad (2.7)$$

where λ_{max1} and λ_{max2} are the successive wavelengths with the maximum reflected light intensity and Φ_{diff} is the phase difference between the two successive wavelengths with the maximum reflected light intensity.

$$\Delta_l = \frac{\lambda_{max1} \lambda_{max2}}{\lambda_{max2} - \lambda_{max1}} \quad (2.8)$$

Plugging (2.3) into (2.6), we obtain,

$$2\Delta d \sqrt{(n^2 - \sin^2 \theta)} = \frac{\Delta_\lambda}{\lambda_s} \cdot \Delta_l \quad (2.9)$$

Then the thickness variation of the sensitive layer can be written as,

$$\Delta d = \frac{\Delta_\lambda \Delta_l}{2\lambda_s \sqrt{(n^2 - \sin^2 \theta)}} \quad (2.10)$$

where Δ_λ can be measured by spectrometer and Δ_l is calculated by equation (2.8).

In the thesis, the measurement results by spectrum shift method are used as reference values to compare with the measurement by the dual-LED method.

2.3.2 Dual-LED Method

The expensive and bulky spectrometer used in the setup for experiments makes the sensor less cost effective. Dual-LED biosensor is proposed to replace the spectrometer in order to reduce the cost and size of the device. The model of variation of the sensitive layer thickness is derived for this approach.

From equation (2.1), we know the ideal interference pattern is a cosine function of wavelength (Figure 2.3), which is different from the real one. The real spectrum is measured and shown in Figure 4.4 and Figure 4.8. So different numerical methods are developed to evaluate the interference pattern. The regression modeling

based on polynomials is adapted to fit the spectrum curve. The profile of the spectrum is assumed as,

$$I'_r(\lambda) = A_1 + B\lambda + C\lambda^2 \quad (2.11)$$

$$I'_{rshift}(\lambda) = A_2 + B(\lambda + \Delta_\lambda) + C(\lambda + \Delta_\lambda)^2 \quad (2.12)$$

where $I'_r(\lambda)$ and $I'_{rshift}(\lambda)$ are reflective beam intensities before and after thickness variation respectively.

Interference from the environment will affect the measurement, so the real spectrum moves up/down. Thus, coefficients A_1 and A_2 are not equal. Here we make an assumption that the shape of the spectrum will not change with a small spectrum shift.

The changes in the reflected intensity of the two LEDs are measured by a photo detector, and calculated by reflected beam intensity change before and after thickness change at each wavelength. Define intensity change for one LED as,

$$\Delta I_1(\lambda_1) = I'_{rshift}(\lambda_1) - I'_r(\lambda_1) \quad (2.13)$$

where λ_1 is one of dual LEDs' wavelengths in the sensor. $I'_{rshift}(\lambda_1)$ is the intensity after binding, $I'_r(\lambda_1)$ is before the binding. The LED intensity change at another wavelength is similar. So the total intensity change is calculated as,

$$\Delta I = \Delta I_2(\lambda_2) - \Delta I_1(\lambda_1) \quad (2.14)$$

where λ_2 is the other wavelength of two LEDs in the sensor.

By inserting (2.11), (2.12), (2.13) into (2.14), we can get the relation between optical path difference variation and reflected intensity change,

$$\Delta I = 2C(\lambda_2 - \lambda_1)\Delta_\lambda \quad (2.15)$$

The spectrum shift measured by dual-LED sensor can be expressed by,

$$\Delta_\lambda = \frac{\Delta I_2(\lambda_2) - \Delta I_1(\lambda_1)}{2C(\lambda_2 - \lambda_1)} \quad (2.16)$$

Because the relationship between spectrum shift and optical path difference

variation is known in equation (2.5), and plugging equation (2.10) and (2.16) into (2.5) we obtain,

$$\frac{\Delta I/2C(\lambda_2 - \lambda_1)}{\lambda_s} = \frac{2\Delta d\sqrt{(n^2 - \sin^2 \theta)}}{\Delta_l} \quad (2.17)$$

Finally, the solution for the thickness change is

$$\Delta d = \alpha \frac{\Delta I_2(\lambda_2) - \Delta I_1(\lambda_1)}{4(\lambda_2 - \lambda_1)\sqrt{(n^2 - \sin^2 \theta)}} \quad (2.18)$$

where $\alpha = \frac{\Delta_l}{C\lambda_s}$, which is the characteristic constant of the sensor chip, measured by the

spectrometer.

Chapter 3 System Design

In this chapter, the bio-agent detection device based on Field-Programmable Gate Array (FPGA) is presented. The functions and structure of the main parts of the system are introduced.

The bio-agent detection device consists of four main parts, which include a dual-LED sensor module, a FPGA board, an interface circuit board, and a power supplier. To realize a handheld device in a credit card size, the circuit based on FPGA is chosen, because it's easy to transfer from the prototype into ASIC design, which is our final target. The wireless communication function is integrated into the system by connecting the dual-LED bio-agent detection system to external wireless module. This function makes the device work as a network sensor, extending the function of the sensor device effectively. The structure of the prototype is shown in Figure 3.1.

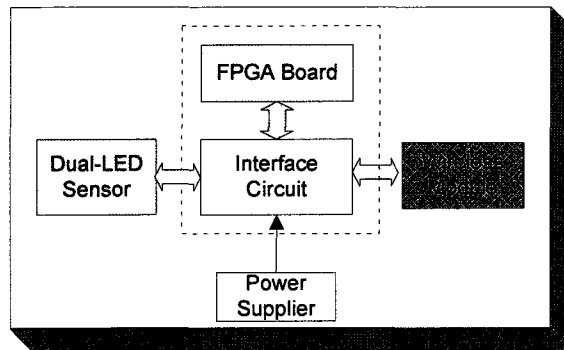


Figure 3.1. Diagram of the dual-LED bio-agent detection system device based on
FPGA

The entire wireless dual-LED bio-agent detection system is composed of several dual-LED bio-agent detection devices with a wireless transceiver, and a work PC with a wireless receiver and a data process application as shown in Figure 3.2. The data

from dual-LED sensor is acquired by FPGA circuit board and then transferred by the wireless module. The work PC receives the sensor data by the wireless receiver, and the data is processed by the application.

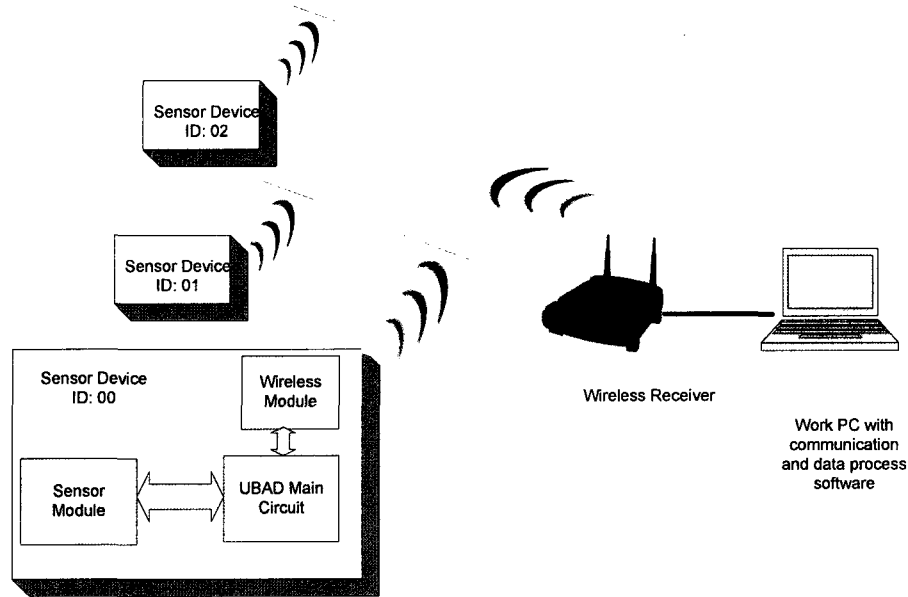


Figure 3.2. Diagram of the wireless dual-LED bio-agent detection system

3.1 Dual-LED Sensor

Sensor module is the most critical part in the dual-LED bio-agent detection system, which mainly determines the performance of the whole device. The sensor is composed of dual LEDs with different wavelengths, one photo detector, and the structure to hold them in a compact size. The schematic diagram and the electrical schematic of the sensor are shown in Figure 3.3 and Figure 3.4 respectively.

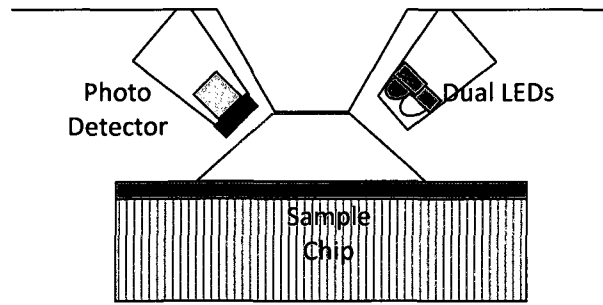


Figure 3.3. Schematic diagram of the measurement system

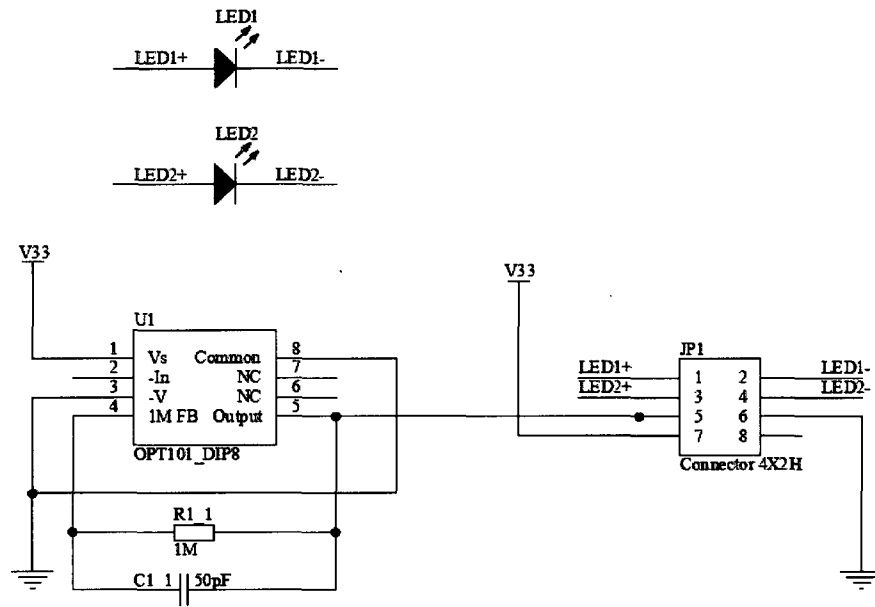


Figure 3.4. Schematic of the dual-LED sensor

Two LEDs are used as the light source in the sensor. The type of LEDs in the sensor is chosen by several parameters. First, one peak or trough of the sensor chip spectrum is chosen to measure the spectrum shift. The wavelengths of two LEDs should be in the range of the both slopes of the peak or trough respectively. After the range of wavelengths are decided, two LEDs are chosen from the commercial products available based on the parameters including peak wavelength, spectral half width, and viewing half angle. Because the sensor chip spectra are different in the two different experiments, the specific LEDs selection is discussed in chapter 4.

To balance the reflected light beams at two different interfaces, the incident angle is decided at 30°. With this incident angle, the LEDs and the photo detector can be installed into the sensor holder easily mechanically. Meanwhile this angle keeps consistent with the setup in previous experiments by the research group to make all the experiments data comparable.

To make the sensor compact and miniaturized, only one photo detector OPT101 (TI, US) is used in the design. It is a monolithic photodiode integrating an on-chip transimpedance amplifier inside the chip, so the output of the detector can be connected to ADC directly. Since an amplification circuit is no longer needed, the size and cost of the sensor can be reduced. Meanwhile, with integration of the transimpedance amplifier on a single chip, the leakage current errors, noise pick-up, and gain peaking due to the stray capacitance can be eliminated effectively. The amplifier uses 3.3 V from interface board as a single power-supply, which makes it ideal for a battery operated equipment. And the detector has high responsivity with 0.45A/W at 650nm, and a wide spectral responsivity range (Figure 3.5), which includes the wavelengths of the LEDs used in the sensor.

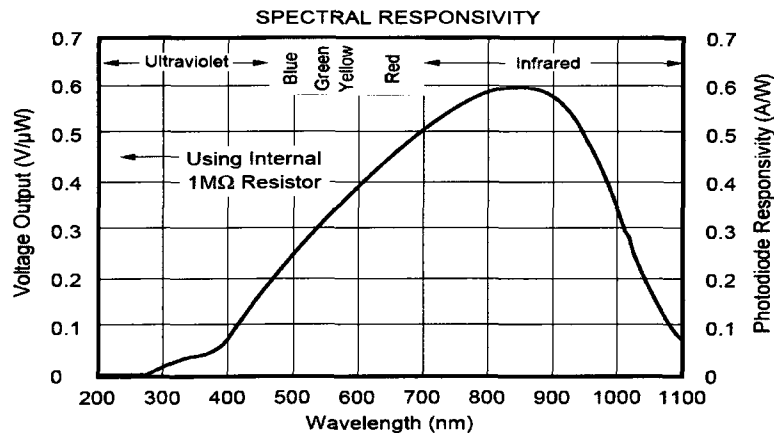


Figure 3.5. Spectral responsivity of the photo detector from the manual of OPT101

3.2 Interface Circuit Board

The interface circuit board bridges the FPGA board, the dual-LED sensor and external wireless module. A user can operate the device by the operation interface, four switches in this design. The interface circuit board displays the numerical result of detection after the measurement. It transmits the acquisition data to the wireless communication module. Meanwhile, it supplies the entire system with the power of single 3.3V.

The interface circuit board is composed of operation interface, sensor control module, data acquisition, display module, communication interface, and power supply module, shown in Figure 3.6.

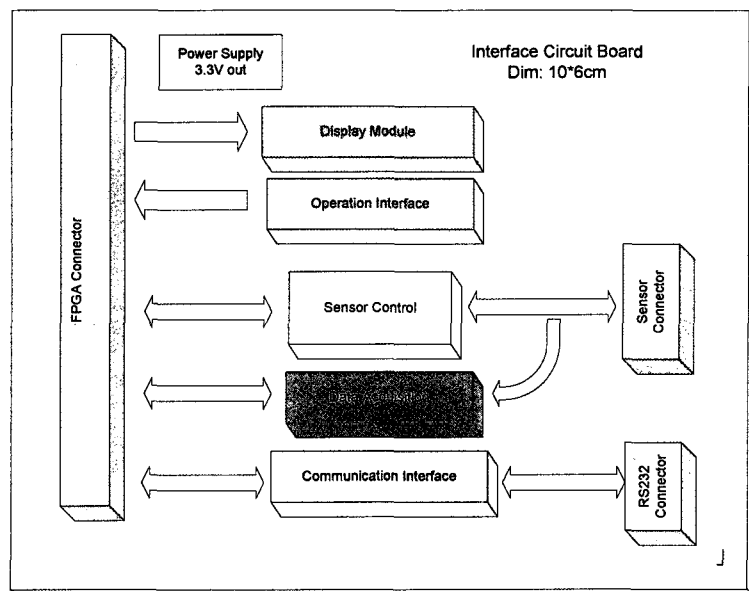


Figure 3.6. Diagram of the interface board

The operation interface, composed of four surface-mounting switches, is used to control the LED beam intensity acquisition. When switch 0 is pressed, the 2 reflected LED beam intensities of the first sample are measured, and switch 1 for the

second sample. While the switch 2 pressed, the system is reset and the registers storing the acquired data are set to 0.

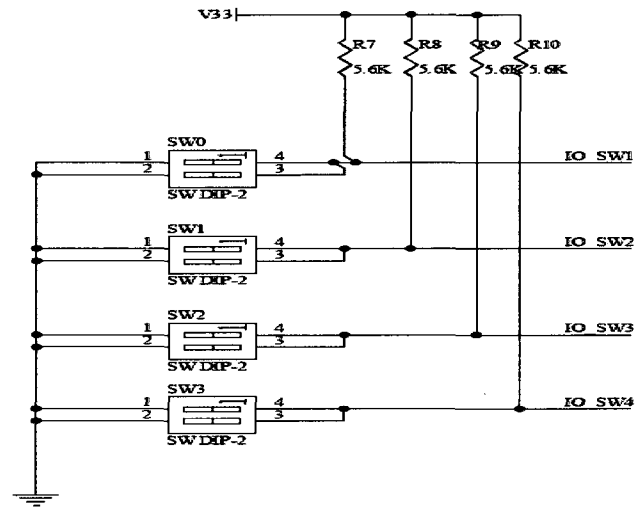


Figure 3.7. Schematic of the operation interface

The sensor control module receives control signal from the FPGA board, then drives dual LEDs in the sensor. An n-channel enhancement mode MOSFET ZXMD63N02 is used as an analog switch. It combines the benefits of low on-resistance 0.13Ω with fast switching speed, which makes it ideal for high efficiency, low voltage and power management application.

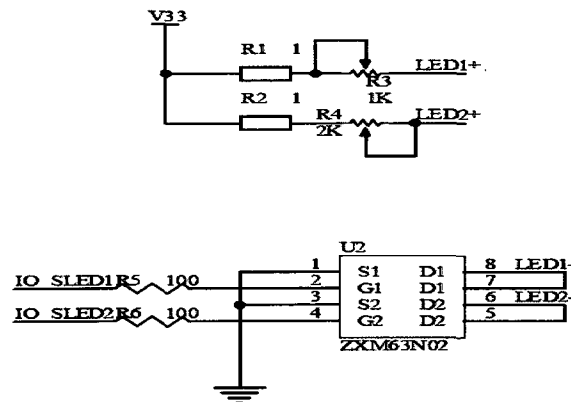


Figure 3.8. Schematic of the sensor control circuit

The data acquisition module consists of an analog-to-digital converter (ADC) and its accessories circuit, which connects to the sensor output and converts the analog signal to the digital signal for the FPGA. The LTC 1863 with 8-channel 12-bit with serial I/O is used as ADC chip in the design. The 8-channel input multiplexer is configured for single-ended inputs and unipolar conversion. The automatic nap and sleep modes make the data acquisition energy-saving, and benefit the design of system, which is power sensitive.

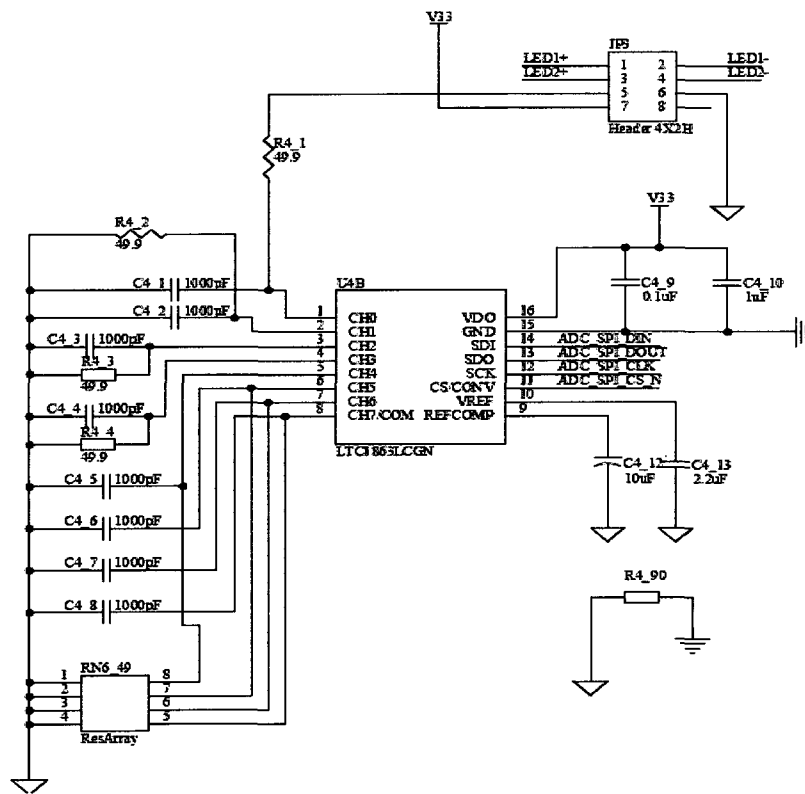


Figure 3.9. Schematic of the data acquisition module

After the reflected intensities of samples are acquired, the display module receives the measurement results from the FPGA board and shows them on three 7-Segment Numeric LED Displays on the interface board. The result is displayed as decimal values.

Four indicator LEDs is controlled by FPGA board, and indicate the working states of the system. When LED indicator1, DS5 is on, the sample 1 measurement is done. When LED indicator2, DS6 is on, the sample 1 measurement is done. LED indicator3, DS7 is used as the reset signal. When LED indicator3 is on, all the data are set to 0, and the process restarts. LED indicator0, DS4 indicates the results of measurement. If LED indicator0 is blinking, the system detects the thickness change on the sample beyond the threshold, which is the minimum thickness change the sensor can detect. If LED indicator0 is off, no significant thickness change is measured. If LED indicator0 is on, an error occurs in the measurement. Operator needs to check the system.

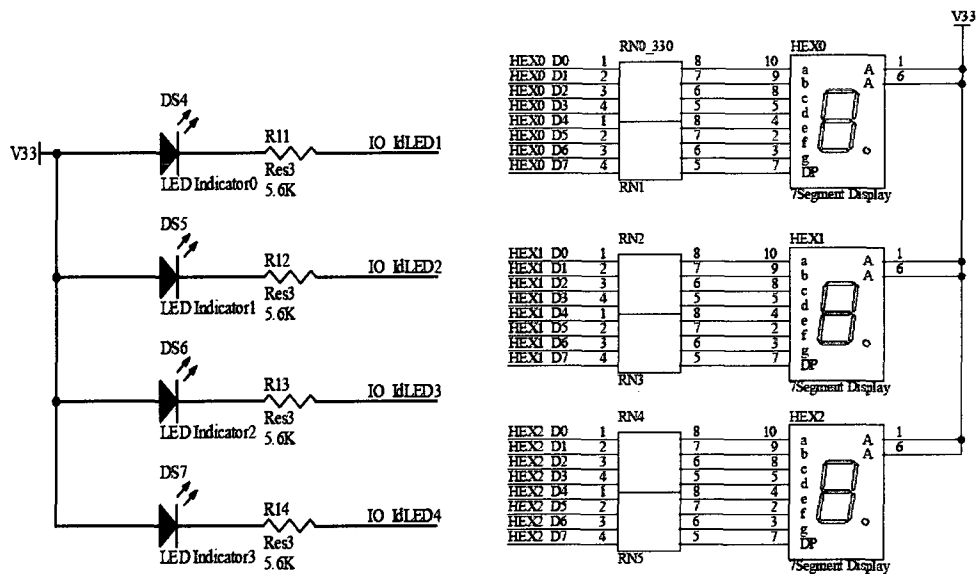


Figure 3.10. Schematic of the module for the results displaying

The communication interface transfers the intensity data measured by the device to the wireless communication module. One MAX3232 device is adopted in the design. It provides the electrical interface between an FPGA asynchronous communication controller and the serial-port connector of the wireless communication module. The device operates at up to 9600 bit/s baud rate with a single 3.3V supply.

LED2 and LED3 are used as indicators for receiving and transmitting data, respectively.

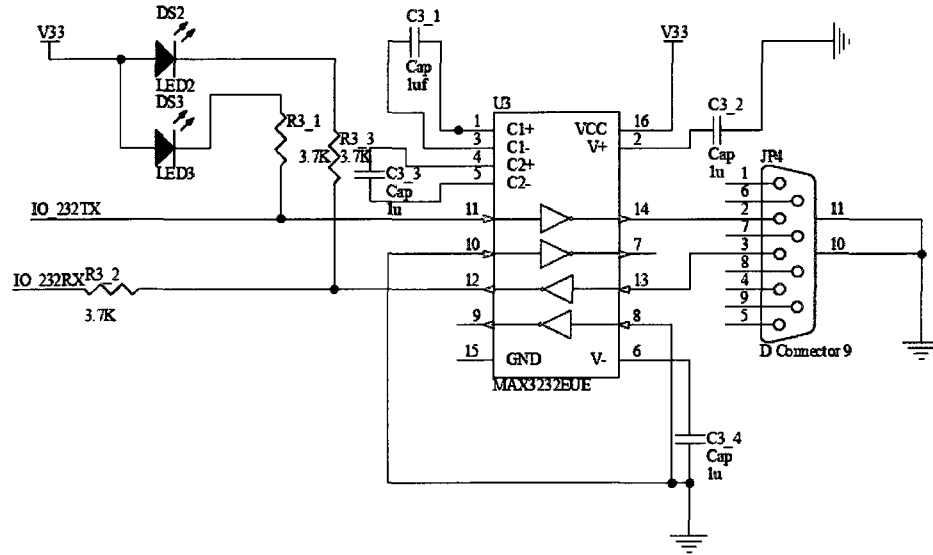


Figure 3.11. Schematic of the communication interface

The power supply module supplies the voltage for the bio-agent detection device. The module uses a positive low-dropout voltage regulator, TLV1117, designed to provide up to 800 mA of output current at 3.3 Volts. A nine-volt battery (PP3 battery), with dimension 48 mm × 25 mm × 15 mm is used as power source and after regulation by the module, it supplies a single 3.3 V for the system power.

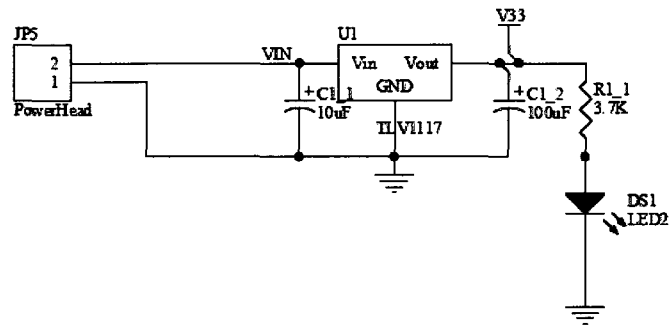


Figure 3.12. Schematic of the power supply

3.3 FPGA Board and HDL Program Design

The FPGA board generates signals to control the data acquisition circuit on the interface board, then reads the data from the sensor by ADC. It processes the data by the method proposed in chapter #2. After the calculation is finished, the results are displayed on the interface board and data are transferred by wireless module.

CMCS002 module board (Dallas Logic Corporation, US) is used as the FPGA board in the design, as shown in Figure 3.13. It includes Altera EP3C25 FPGA, 512K X 8 SRAM, EP1S16 FPGA serial loader (FPGA and Nios II boot), and USB 2.0 Peripheral Port. It supports the specification of master or slave standard card (128pin), providing the interface to extend the external circuit. The FPGA board allows implementation of general logic functions according the requirements of the design. So it is chosen to integrate into design to build up the prototype.

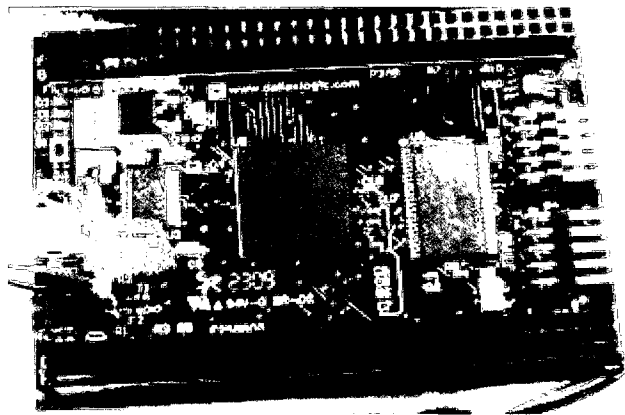


Figure 3.13. CMCS002 module FPGA board

The program for FPGA is designed by hardware description language (HDL), and compiled by Quartus II Web Edition (Altera, US). Quartus II is an effective software tool for analysis and synthesis of HDL designs, which enables the developer to compile designs, perform timing analysis, examine RTL diagrams, simulate a design's reaction to

different stimuli, and configure the target device with the programmer. The HDL program is composed of 6 main parts, which are system synchronizer, sensor LED controller, ADC controller, data processing module, results display module, and wireless communication module (Figure A.2). The pin assignment of the system is listed in Table A.1.

3.3.1 System Synchronizer

System synchronizer module generates synchronous signals for the system running. It coordinates the sensor LED controller, ADC controller, data processing module, results display module and wireless communication module to make them work properly.

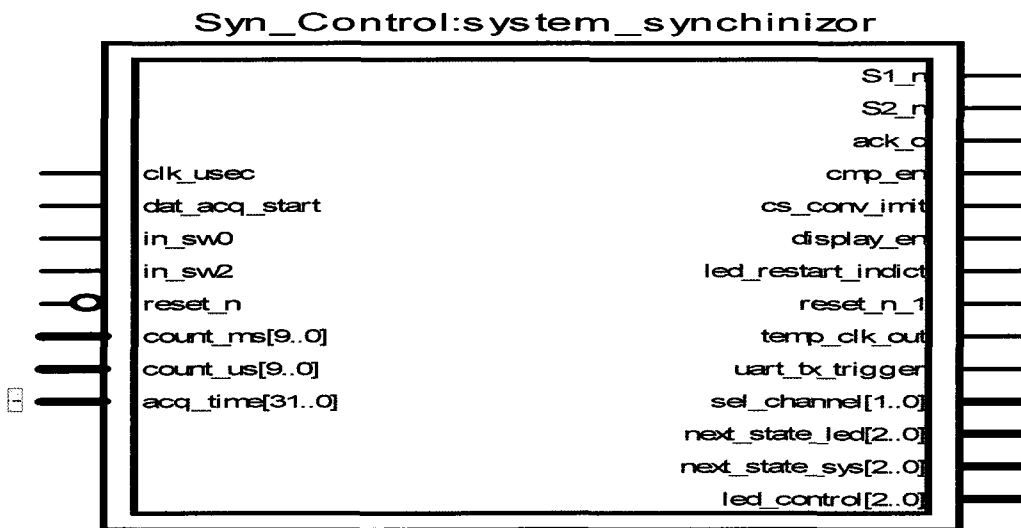


Figure 3.14. Diagram of system synchronizer

Table 3.1. Signal definition of system synchronizer

Signal	Direction	Function
clk_usec	Input	The 1M Hzclock signal for this module.
reset_n	Input	Reset signal from switch 3 on the user interface board. When the “reset_n” is triggered, all the control signals are set to default value.
in_sw0	Input	Input signal of switch 0, active low.
in_sw2	Input	Input signal of switch 1, active low.
count_ms	Input	Microsecond counter.
count_us	Input	Millisecond counter.
dat_acq_start	Input	The pulse signal when the data acquisition begins.
sel_channel	Output	The variable which indicates what type of the intensity is acquired by ADC.
cmp_en	Output	The enable signal for comparison result indicator LE.
display_en	Output	The enable signal for measurement results display.
uart_tx_trigger	Output	Signal to trigger the transmission of the data.
next_state_led	Output	LED state variable.
S1_n	Output	The acknowledgment signal to LED (DS5) to signify sample 1 acquisition is completed.
S2_n	Output	The acknowledgment signal to LED (DS6) to signify sample 2 acquisition is completed.
led_restart_indict	Output	The acknowledgment signal to indicator LED (DS7) on interface board to signify new sampling operation started.

temp_clk_out	Output	The signal to start the ADC conversion.
next_state_sys	Output	The system state variable.
acq_time	Input	Generate reset signal for ADC control module.
ack_o	Output	The signal used to synchronized with led_controller.
cs_conv_imit	Output	The pulse signal at end of sampling to control the LED state from initial state to LED1 state.
led_control	Output	The signal to control the LEDs in the sensor.

3.3.2 Sensor LED Controller

The sensor LED control module is used to generate the signal to control the LEDs in the sensor.

Only one photo detector is used in the sensor setup. In order to measure the intensities of two LEDs in the sensor by one photo detector, a time-division multiplexing (TDM) technique is employed in the design. The two LEDs are controlled to switch on and off respectively at 1Hz frequency and the photo detector is triggered when either one of the LEDs is switched on simultaneously. The output signal from the detector is demultiplexed by electrical circuits. By this method the power consumption is reduced. It not only makes the sensor structure compact, but also reduces the whole system energy consumption.

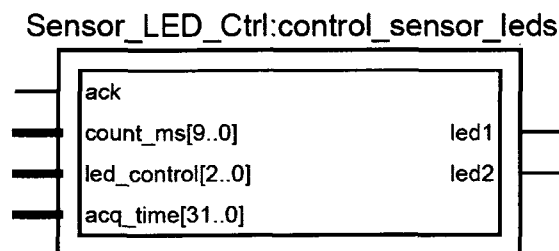


Figure 3.15. Diagram of the sensor LED control module

Table 3.2. Signal definition of sensor LED control module

Signal	Direction	Function
count_ms	Input	A ten bits millisecond counter which is generated by system synchronizer module. It counts the time offset of sampling process in millisecond.
led_control	Input	State variable from system synchronizer module to synchronize the LED control signal.
ack	Input	Indicator of which number of the sample is being sampled.
acq_time	Input	The input generic variable set for the top module, with default value of 100.
led1_sensr	Output	The driver signal for LED1 in the sensor.
led2_sensr	Output	The driver signal for LED2 in the sensor.

When “led_control” is equal to “001” and “ack” is ‘0’ during first sampling process, or “010” and “ack” is ‘1’ during the second sampling process, the first LED in the sensor is powered up for “acq_time”+10 ms after the sampling process is triggered. After the 500ms, the second LED is switched on for the same period as the first LED. During the period when the LED is on, the data acquisition for the reflected LED beam intensities is triggered separately. The time when the LEDs are on is reduced dramatically by this method. If the sensor is measured continuously, it takes only 22% of the whole working time.

3.3.3 ADC Control Module

The ADC interface module generates signals to control the ADC on the

interface board and transfers the sampling data from dual-LED sensor to both FPGA data processing module, and wireless communication interface module.

Table 3.3. Signal definition of the ADC interface

Signal	Direction	Function
clk	Input	The system clock, which is 25MHz on the CMCS002 FPGA board. All the sub-modules are synchronized to this signal.
reset_n_usrint	Input	Reset signal from user interface to stop and start data acquisition.
global_reset_n	Input	The global reset signal, used to reset the system on the board. It's active LOW and asserted by operator.
SDI	Input	Serial data from the ADC chip. It is connected to Pin 13 (SDO), which is the digital data output.
sel_channel	Input	The signal to make ADC to enter SLEEP mode or release from SLEEP mode. Status in SLEEP mode makes the system energy saving.
cs_conv	Output	Used to initiate conversions on the ADC.
sck	Output	Shift clock, which synchronizes the serial data transfer between ADC and FPGA board.
SDO	Output	Used to transfer configuration word from FPGA board to ADC.
data_out	Output	The acquired data from ADC in 12 bit binary format.

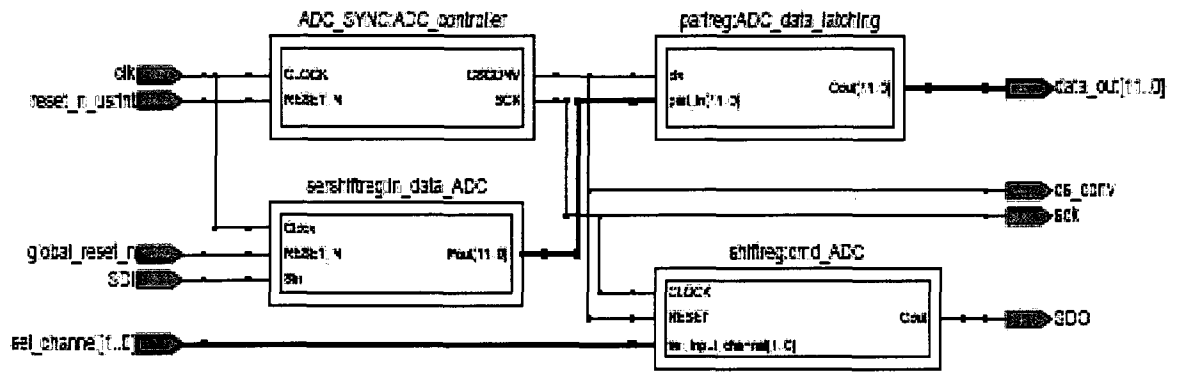


Figure 3.16. Block diagram of the ADC interface

3.3.4 Data Processing Module

The data processing module calculates the thickness variation of the sensor chip sensitive layer by the LED intensities acquired. After calculation of the thickness change, the module compares the results with the threshold value. Based on the comparison, the module drives the indicator LED, “DS0” on the interface board in different mode. If the indicator LED is flashing, variation beyond the threshold is measured. The indicator LED indicates the thickness change of the sample chip is significant. When the indicator LED is switched on, there is an error. When the indicator LED is shut off, there is no significant thickness variation detected.

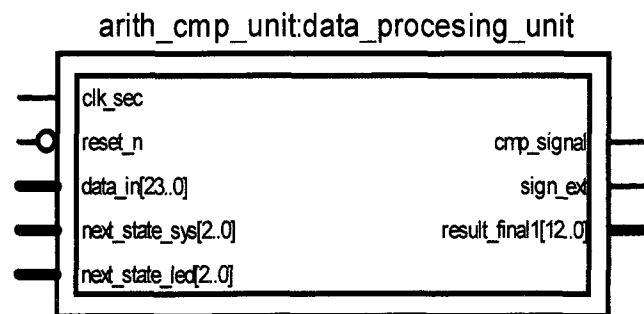


Figure 3.17. Diagram of the data processing module

Table 3.4. Signal definition of the data processing module

Signal	Direction	Function
reset_n	Input	Reset signal from switch 3 on the user interface board.
data_in	Input	Input data for processing. The 0-11 bits are the intensity of the LED 1 , and the 12-22 bits are the intensity of the LED 2.
ctrl_next_state	Input	State variable used as synchronizing signal from system synchronizer module
next_state_led	Input	State variable used as synchronizing signal from system synchronizer module.
clk_sec	Input	The signal to flicker the indicator LED when the thickness variation measured is beyond threshold.
cmp_signal	Output	Used to drive the indicator LED.
result_final1	Output	The calculation result by the module. The results is shown by the results display module on the 7 segments display.
sign_ext	Output	The signal to indicator the sign of the calculation results. If “sign_ext” is ‘1’, the result is minus.

3.3.5 Results Display Module

The calculation result of the thickness difference is shown by three 7-Segment Numeric LED Displays on the interface board.

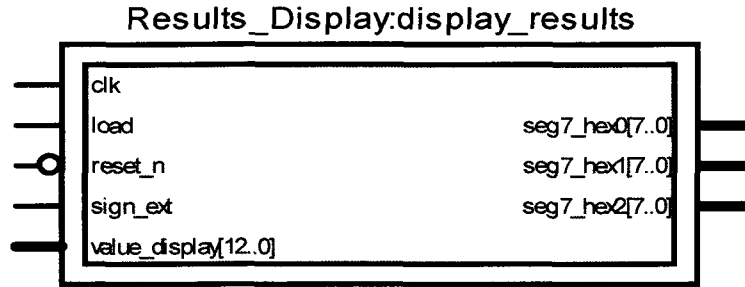


Figure 3.18. Diagram of the results display module

Table 3.5. Signal definition of the results display module

Signal	Direction	Function
clk	Input	The 48MHz clock signal from PLL.
load	Input	The signal to load the value to display when it becomes from low to high.
reset_n	Input	Reset signal from switch 3 on the user interface board. When the “reset_n” is triggered, the value display on the 7-Segment Displays is set to “000”.
sign_ext	Input	The sign of the result.
value_display	Input	The calculation result of the thickness difference, which is from ‘data processing module’.
seg7_hex0	Output	The first 7-Segment Display, which is the lowest significant digit of the result in decimal.
seg7_hex1	Output	The second 7-Segment Display.
seg7_hex2	Output	The third 7-Segment Display, which is the most significant digit of the result in decimal.

3.3.6 Wireless Communication Module

Wireless communication module receives the data from data processing module and transmits them to external circuit after the trigger signal is activated, which is

generated by system synchronizer.

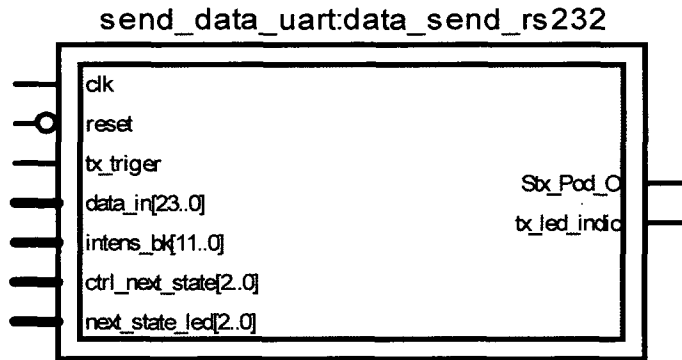


Figure 3.19. Diagram of the wireless communication module

Table 3.6. Signal definition of the wireless communication module

Signal	Direction	Function
clk	Input	The 48MHz clock signal from PLL.
reset	Input	Reset signal from switch 3 on the user interface board.
tx_triger	Input	The signal to trigger transmitting sampling data of the reflected beam intensities.
data_in	Input	The 24 bits input data to be transmitted. 0-11 bits are the intensity of LED 1, and 12-23 bits are the intensity of LED 2.
intens_bk	Input	The background light intensity of the atmosphere measured by the sensor photo detector.
ctrl_next_state	Input	State variable used as synchronizing signal from system synchronizer module.
next_state_led	Input	State variable used as synchronizing signal from system synchronizer module.
Stx_Pod_O	Output	Transmission pin, which transmits the input data in serial.
tx_led_indic	Output	The output signal, which indicates the state of transmitting data by RS 232 interface.

When the sampling process is finished, “tx_trigger” is driven high. Then the “tx_data_cnt”, the counter for the data transmitted is given by 9, which is the total number of the data packet. When state variable “next_state_led” comes into to initial state, “tx_trigger” is driven low. The sampling data are transmitted in serial by packet format shown in Figure 3.20. Each packet consists of 9 bytes data.

Frame Head	Device ID	Sample No. &Data Length	8-11 bit of LED1 intensity	0-7 bit of LED1 intensity	8-11 bit of LED2 intensity	0-7 bit of LED2 intensity	8-11 bit of background	0-7 bit of background
------------	-----------	-------------------------	----------------------------	---------------------------	----------------------------	---------------------------	------------------------	-----------------------

Figure 3.20. Data packet format

Byte 1: Frame head.

The byte is used as identity of the beginning of the packet. When the data packet is sent, it’s the first byte to be transmitted. In our application the framed head is given by 0XF7.

Byte 2: Device ID.

Device ID byte is used to identify the Device in the wireless sensor network. There are multiple sensors in the wireless network, and each sensor is assigned a unique number. The work station can discern which device the data packet comes from. In our application, the maximum number is 128.

Byte 3: Sample No. and data length.

This byte is divided by 2 parts, which are composed by 4 bits separately. The first part (4-7 bits) is used as the sample sequence number. The second part (0-3 bits) is bytes number of the intensity data to be transmitted.

Byte 4: 8-11 bits of LED1 intensity.

0-3 bits of this byte carry the value of 8-11bits of the LED1 intensity. The

bits left (4-7 bits) are given by 0X00.

Byte 5: 0-7 bits of LED1 intensity.

This byte is given by the value of 0-7 bit of the LED1 intensity.

Byte 6: 8-11 bits of LED2 intensity.

0-3 bits of this byte carry the value of 8-11bits of the LED2 intensity. The bits left (4-7 bits) are given by 0X00.

Byte 7: 0-7 bits of LED2 intensity.

This byte is given by the value of 0-7 bit of the LED2 intensity.

Byte 8: 8-11 bits of background intensity.

0-3 bits of this byte carry the value of 8-11bits of the background intensity.

The bits left (4-7 bits) are given by 0X00.

Byte 9: 0-7 bits of background intensity.

This byte is given by the value of 0-7 bit of the background intensity.

3.4 Casing Design and Fabrication

3D printing, a form of additive manufacturing technology, is employed to fabricate the system casing prototype. The object in three dimensions is created by successive layers of material. As a tool for creating models early in the design process, 3D Printing, which reduces the design cycle effectively, is a faster and more affordable alternative to Rapid Prototyping technology. For our application, the casing fabrication can be finished within 1-2 days. And the printer uses acrylonitrile butadiene styrene (ABS) plastic as printing material so the cost of the model is inexpensive. Advanced 3D printing technologies produce models, and they can emulate the appearance, and functionality of

the final design.

The model is designed using Prof-E software. The STL file of the design, which is input format used by 3D printer is stored. Dimension 1200 SST 3D Printer by Stratasys, Inc. is used in our design. The design file in STL format is loaded into machine, and the printer fabricates the model layer by layer according the input file. After finishing printing, the model is put into the solution to dissolve the support material.

The model for the system includes three parts, a sensor holder, a body case and a panel cover, as shown in Figure 3.21. The sensor holder holds the LEDs and the photo detector, and makes the incident and reflective angle both at 30° . The body case is used to hold the main circuit boards including the interface board and FPGA board. The panel cover is used to cover the body case, and the holes in different sizes on the cover make the operation button and results display component exposed to the user.

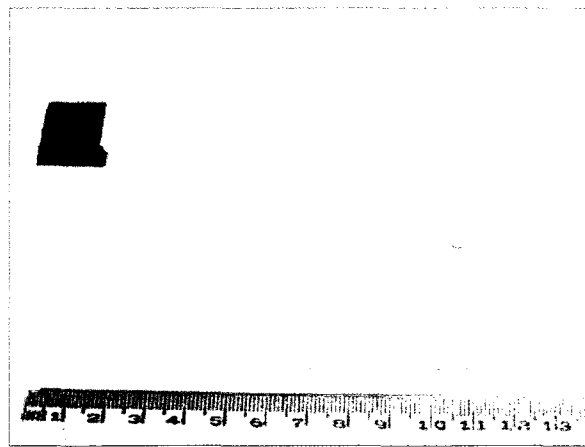


Figure 3.21. Picture of the casing

3.5 External Wireless Communication Module

PN2400 wireless module (Linxsia LLC, US) is used as the external wireless module in the system. PN2400 wireless module is a wireless transceiver in small size with lower power consumption. The transmit power output is 1mW, when it's working in

transferring data continuously. The module is powered up by 3.3V DC, which is the same as the supply voltage to the main FPGA. When integrating the wireless module into the dual-LED bio-agent detection device, no extra voltage regulator circuit is needed. The communication interface between the main board and PN2400 is connected by 3-wire 3.3V RS-232 interface, which are transmitting, receiving, and ground pin. The PN2400 is integrated with 3.3V RS-232 transceiver, so the hardware for communication on FPGA board is only a RS-232 converter chip. The data from the sensor is sampled at 1Hz. The data rate is at about 8bytes/s, which is much lower than the RF data rate of the wireless module, which is 250K bps. The characteristics describing above make PN2400 meet the requirements of the dual-LED bio-agent detection wireless system.

3.6 Application Design for Work PC

The application receives the data from the biosensor device and shows the processing results to operators (Figure 3.22).

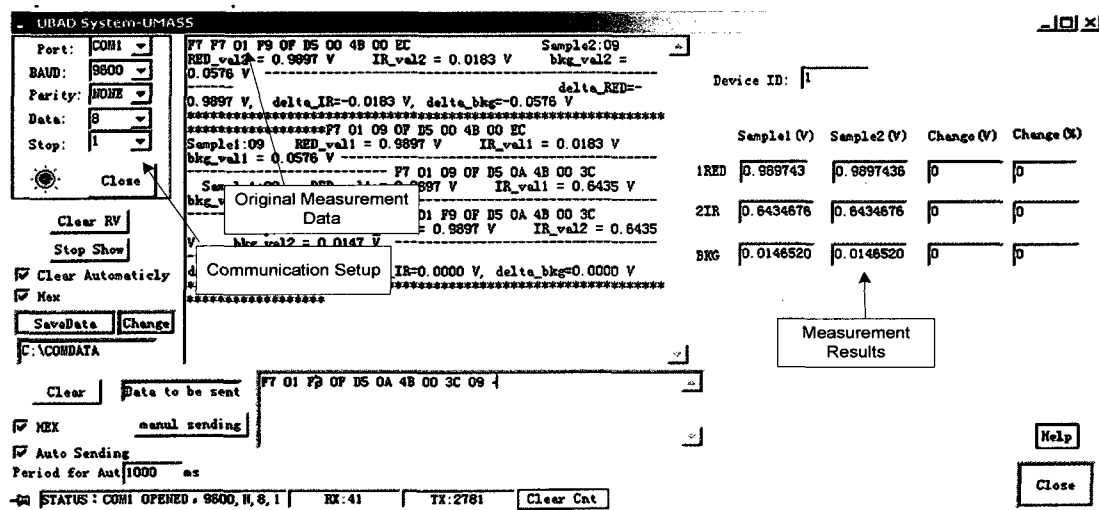


Figure 3.22. PC Application for data receiving and processing

A wireless receiver connects work PC by internet cable, and receives the real-time data acquired by biosensor device in the network. Then the application reads the

data from wireless receiver, processes them and shows the results on the screen finally.

The application is designed by Visual C++ (Microsoft Inc. US).

Chapter 4 Results and Discussion

To verify the model for thickness change measurement and test the FPGA sensor device, two types of experiments are designed in the project. The sensor chip samples are measured and the data is processed by the bio-agent detection system based on FPGA. Finally the results are compared with the ones by spectrum shift method.

4.1 Experiments

The experiments are carried out by prototype of the bio-agent detection system (Figure 4.1). The sample chips are scanned by dual-LED sensor (Figure 4.2) on the device and the data is processed by the system.

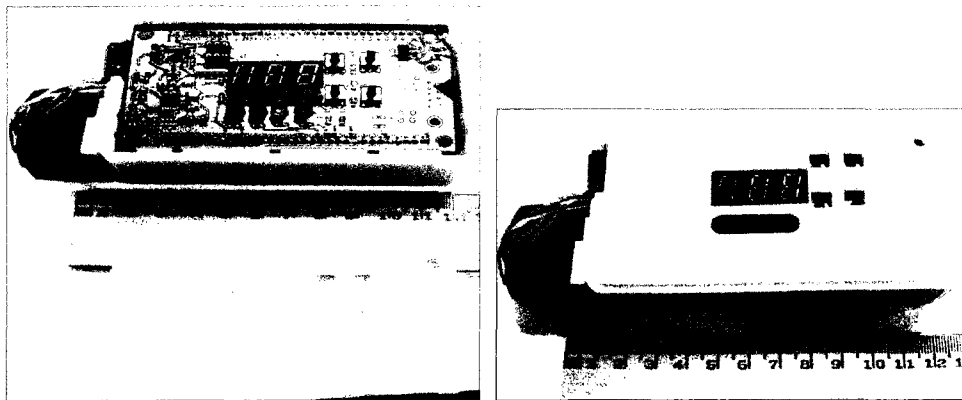


Figure 4.1. Pictures of the system prototype



Figure 4.2. Picture of the sensor holder part

In the first experiment, the sample sensor chips with different oxidized silicon layer thickness at both sides are used. The thickness difference on one sensor chip simulates sensitive layer changes on the real sensor chip introduced by the bio-reaction binding. With these samples the model and device can be tested with a larger range of the thickness variation. In the second experiment, the dual-LED sensor coupled with a functional PMMA thin film coated onto an oxidized silicon wafer is tested. The thickness variations caused by recombinant Protein G' binding to the PMMA layer with different incubation time are measured.

4.1.1 Experiments with Sample Chips with Step Difference

In this experiment, we focus mainly on verifying the thickness variation evaluation. Sensor chips 10×18mm with different thickness at both sides are fabricated, as shown in Figure 4.3. First, a silicon wafer with 500μm thickness silicon dioxide (Ultrasil Corporation, US) is patterned and diced. Then one side of the sample chip is etched to make the step difference. Six sample chips with thickness difference from 2-20nm are fabricated for the experiments.

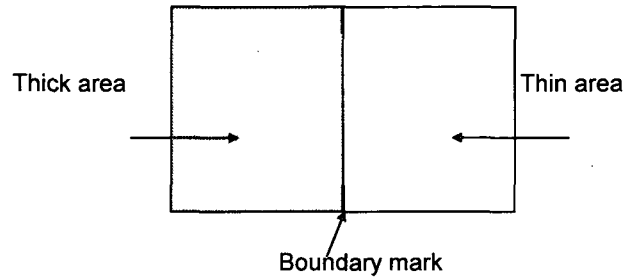


Figure 4.3. Sample diagram

Sample spectrum is measured by a spectrometer (USB4000, OceanOptics, US) at 30° incident angle, which is consistent with dual-LED sensor device setup. Figure 4.4 depicts two different spectra for samples with two different thickness variations. It is clear from the graphs that the spectrum shift is proportional to the thickness variation. According to the spectrum profile, two wavelengths at both sides of the peak wavelength of the spectrum are picked to choose the proper type of LEDs, 590 nm and 780 nm, as shown in Figure 4.4 (a). In this experiment, two LEDs with 590nm center wavelength (LED591E, Thorlabs, US) and 780nm center wavelength (LED780E, Thorlabs, US) are used.

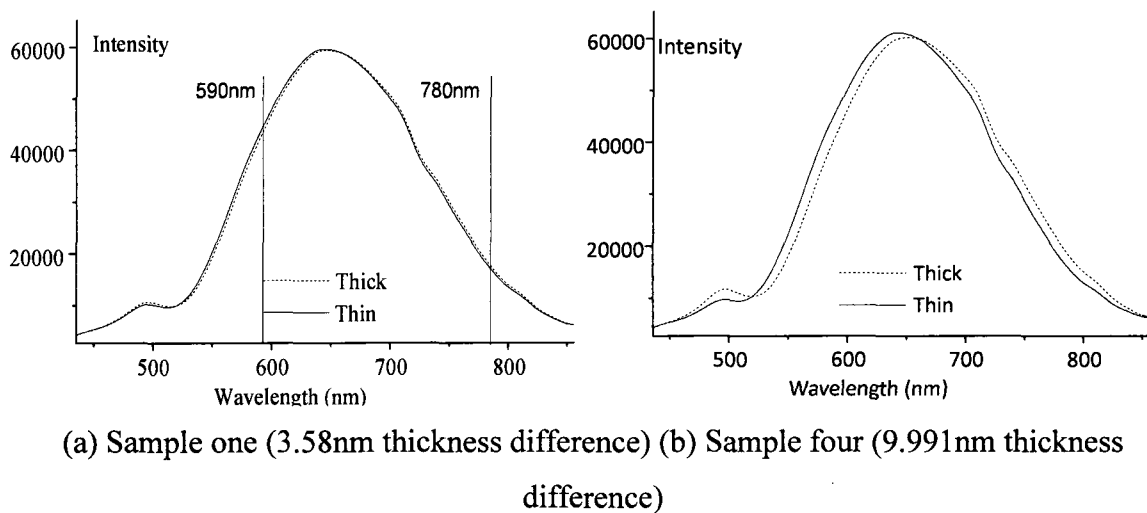


Figure 4.4. Spectrum and spectrum shift of different sample chips

After deciding the wavelengths and types of LEDs employed in the sensor device, the frequency range from 555nm to 795nm is chosen to fit the spectrum profile. The regress modeling based second order polynomials is adapted. By using a Matlab program, parameter C in equation (2.11) can be calculated out.

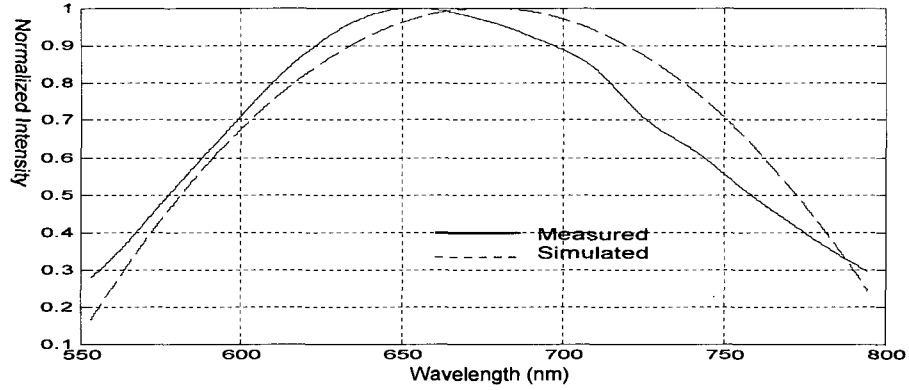


Figure 4.5. Normalized spectrum profile and simulated spectrum by second order polynomials

Samples are scanned by the dual LEDs sensor from the thin to the thick area. Figure 4.6 shows the intensity change along with position for sample 3. This variation comes from the inference pattern change that is caused by the thickness change of the silicon oxide layer at both sides. If the thickness of the thin film layer is constant, stable intensity can be acquired. From the experimental results we find that the reflected beam intensity is stable at both thin and thick areas. When the light beams move out of the sample surface, a significant drop can be measured by the photo detector as shown at the left and right edges in Figure 4.6. This experiment verifies that the thin film surface is uniform at each side, and is sufficient to perform the thickness variation measurement. It also helps to locate the best range to make the measurement. For sample 3, we choose position 7 and 15 as the measurement points.

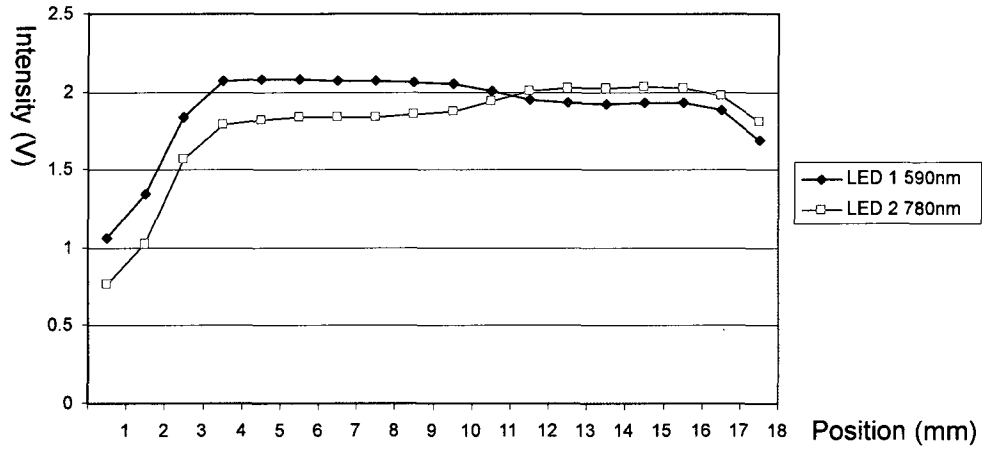


Figure 4.6. Intensity variation along the sample three chip

In this experiment, six silicon chips with silica thin film layer are used as sample chips. Thickness changes measured by dual-LED sensor and by spectrum shift method are listed in Table 4.1 and plotted in Figure 4.7.

Table 4.1. Measurement results of the thickness variation for the first experiments

Sample NO. / Method	1	2	3	4	5	6
Spectrum shift (nm)	3.580	4.24	5.811	9.991	10.846	13.392
Dual-LED (nm)	4.239	4.751	6.715	10.057	11.772	16.314

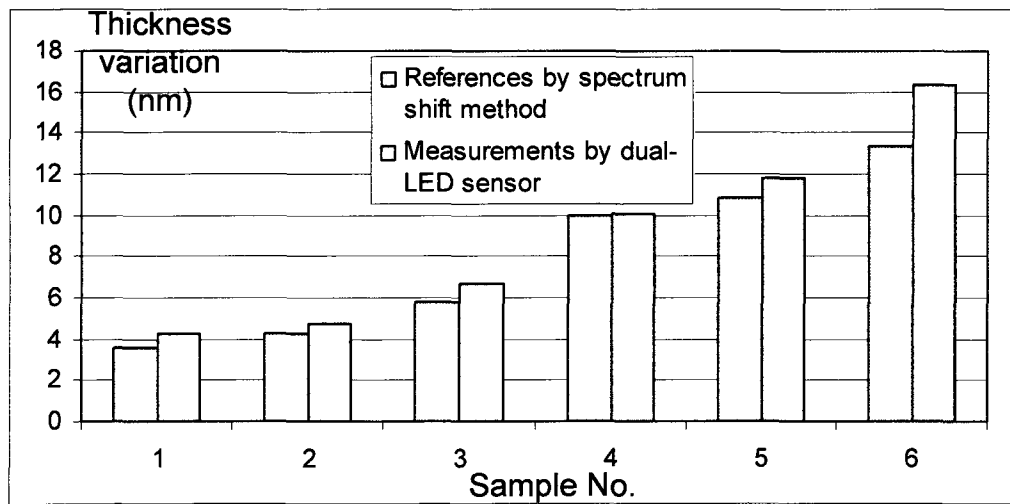


Figure 4.7. Thickness variation measured by the dual LEDs sensor and spectrum shift method

4.1.2 Experiments with Protein G' Binding

In order to simulate the real situation, the second experiments are made by binding Protein G' on the PMMA biomaterial layer, resulting in a shift in the reflection spectrum due to the increase in sensitive layer thickness.

The sample spectrum is measured by spectrometer at 30° incident angle by the same procedure as in the first experiments. The spectrum of the sample is as shown in Figure 4.8. Based on the spectrum data, the sensor adopts the LEDs with peak wavelengths at 590nm and 700nm as light source for the experiments. Then the frequency range from 585nm to 715nm is chosen to fit the spectrum profile, as shown in Figure 4.9. The regress modeling based on the second order polynomials is adapted to calculate the parameter C in equation (2.11).

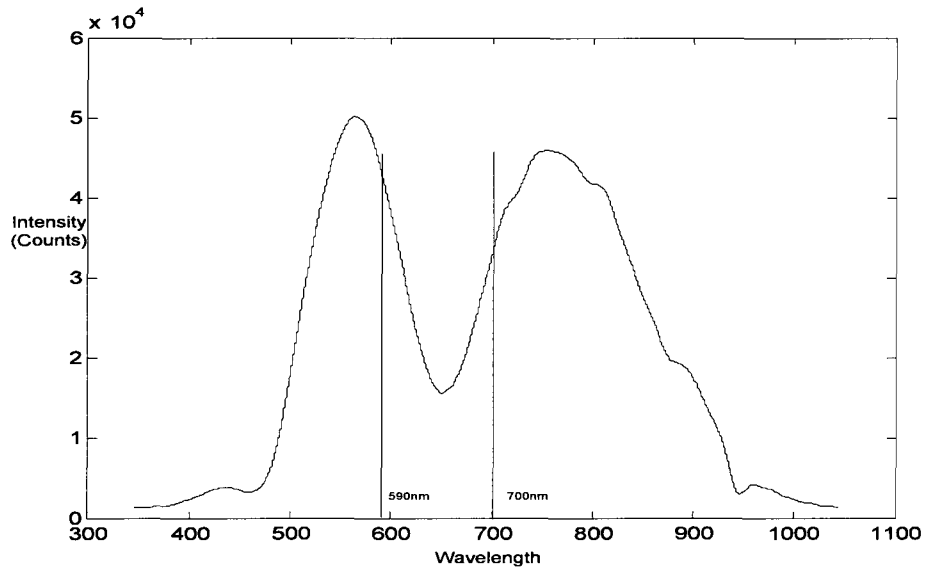


Figure 4.8. Spectrum of the sample with a PMMA layer

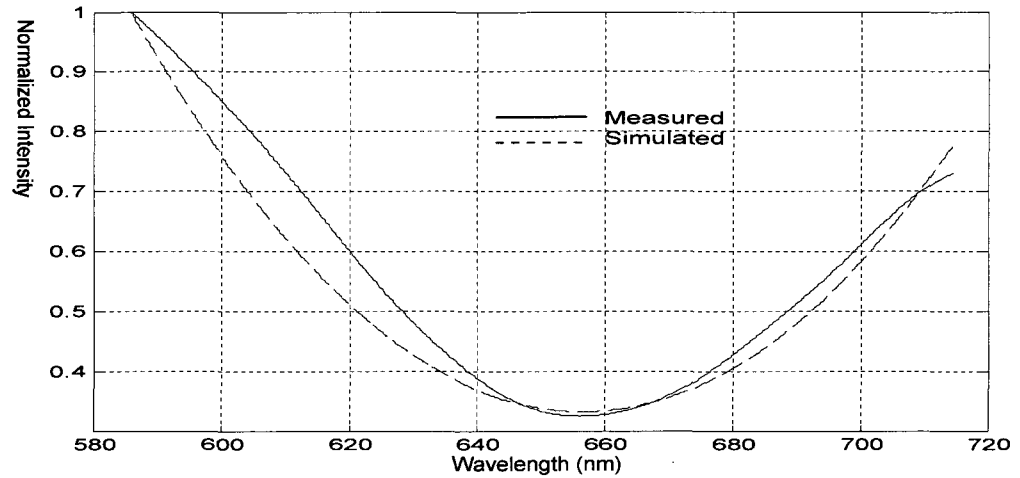


Figure 4.9. Spectrum profile and simulated spectrum by second order polynomials for biochips with a PMMA layer

The experiments are made by the bio-agent detection system with FPGA circuit board to acquire the data and process them. Firstly, the blank chip is attached to the stage on the case and the chip is measured by the dual-LED sensor and spectrometer without any biomaterial on it. Secondly, 200 μ L protein G' (20 μ g/mL) is placed on the chip surface and then the protein G' is incubated for a half hour under room temperature. When the incubation is over, the protein G' is rinsed off with water and the chip surface is dried with an air blower. Then the chip is scanned by dual-LED sensor. Finally, the spectrum is measured to make comparison with the measurement results by dual-LED sensor.

In this experiment, three sensor chips with PMMA thin film layers are used as sample chips to measure the thickness variation caused by protein G' binding. From normalized spectrum of sample three, we can observe the spectrum shift clearly (Figure 4.10). The thickness changes are measured by both approaches and the measurement

results are compared, as listed in Table 4.2 and plotted in Figure 4.11.

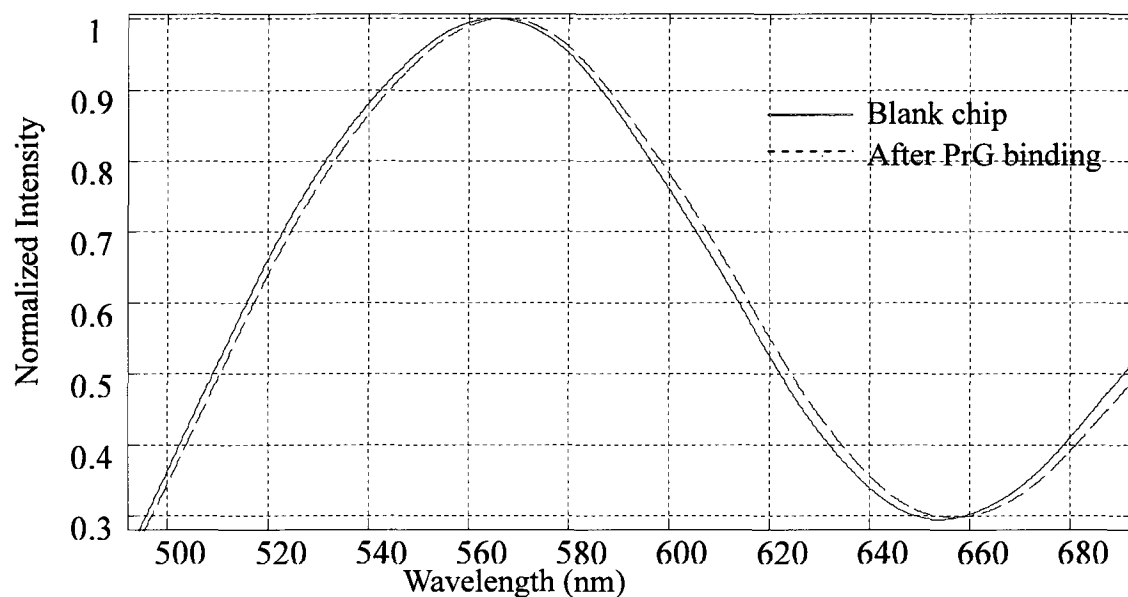


Figure 4.10. Spectrum of sample three

Table 4.2. Measurement results of thickness variation for the second experiments

Sample NO.	1	2	3
Method			
Spectrum shift (nm)	0.718	1.921	2.773
Dual-LED (nm)	1.828	1.991	3.378

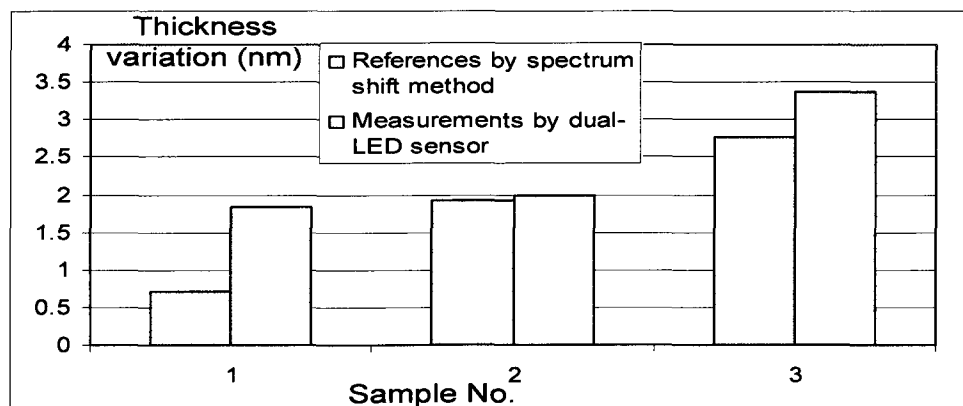


Figure 4.11. Thickness variation measured by the dual LEDs sensor and spectrum shift method

4.2 Discussion

The experiment results indicate that the trend of thickness variations measured by dual LEDs agrees with the values obtained by spectrum shift method.

In the first experiment results in Figure 4.7, the bio-agent detection system with the FGPA estimates the thickness difference on the sample chips. The system with the proposed model works well to measure the sample with thickness difference between 4 nm to 10 nm. From the second experiments results in Figure 4.11, the system measures the thickness change by the bio-reaction binding well in the range from 2 nm to 4 nm in the experiments.

However, the system overestimates around 25% compared with the reference for the sample six with 13.40nm thickness difference in the first experiments. It shows a big error in measuring the sample with lower than 1nm thickness change in the second experiments. The factor of the overestimation in the first experiments is that the mathematical model for the thickness change is made based on a small spectrum shift which is caused by a small thickness change of the sensitive layer. Within a rational range 4-10 nm of the change, the model works well. On the other hand, when the thickness change is too small, the noise from the atmosphere overwhelms the wanted signal. Thus, the accuracy of the measurement results can't be guaranteed. The noises mainly come from the photo detector, which will be affected by the light from the atmosphere. And the resolution of the ADC also affects the accuracy of the measurement. From the second experiment results, there is an error from the sample with less than 1 nm change.

Chapter 5 Conclusions

In this thesis, the model to estimate the sensitive layer thickness variation on the sensor chip was analyzed for two different methods. One was the spectrum shift method, which was used as a reference. The other was dual-LED sensor measurement.

A new design of the bio-agent detection system was presented. The bio-agent sensor device consists of four main parts, a dual-LED sensor module, a Field-Programmable Gate Array (FPGA) board, an interface circuit board, and a power supplier. The LEDs' signal is converted into digital data by the interface board and processed by the FPGA board. The measurement results are shown by the interface board. And the device is powered by a nine-volt battery, which enables portability of the device. Meanwhile, the wireless communication module is integrated into the bio-agent detection system to operate as a network sensor. The prototype using the Altera Cyclone III FPGA chip as the main processor core was built. The basic functions of the software of the FPGA board were realized, including the data collection and transmission. However, the power consumption of the system is still relative high. The sensor device works around six hours at 100 milliamperes continuously with one battery.

The measured values by the dual-LED sensor were compared with their reference values by the spectrum shift method within the range from 2 to 15 nm. The results indicate that the trend of thickness variations measured by dual LEDs agrees well with the reference values. However, a bigger error occurs when the thickness change goes beyond the rational range, 15nm thickness change. For a small thickness change smaller

than 1 nm, there is a noise issue. The noises mainly from the ADC and the photo detector, which will be affected by the light from the atmosphere, limit the minimum thickness change that the sensor device can detect.

From the experiments, the handheld device for the biosensor becomes practical by this method using dual LEDs and a photo detector with the FPGA circuit based on the reliable model.

RECOMMENDATIONS

The model validated in this thesis is applicable to an optical biosensor with a transparent sensitive layer based RIfS. This model assumes that a small thickness change happens during the measurement. For further work, a more precise model should be studied to extend the range for the detection.

To improve the accuracy, LEDs, photo detector, and the structure holding them should be optimized to reduce the noise introduced in the measurement. The high order of polynomials, which fit better to the measured spectrum in overall range, will improve the estimation.

The size of the system can be optimized further by integrating LED and photo detector into one device using micro-machining technology. In addition, the circuit board can be designed by ASIC. The HDL program for FPGA board in the current program can be easily transferred to the ASIC design. For the wireless communication, the smaller module should be used to replace the one employed in the current design. In this way, the whole device can be implemented in a credit-card-size, which is our final target.

More experiments need to be made to exam the relationship between the thickness change and the incubation time. It would help to understand the characteristic of the sensor chip.

APPENDIX A

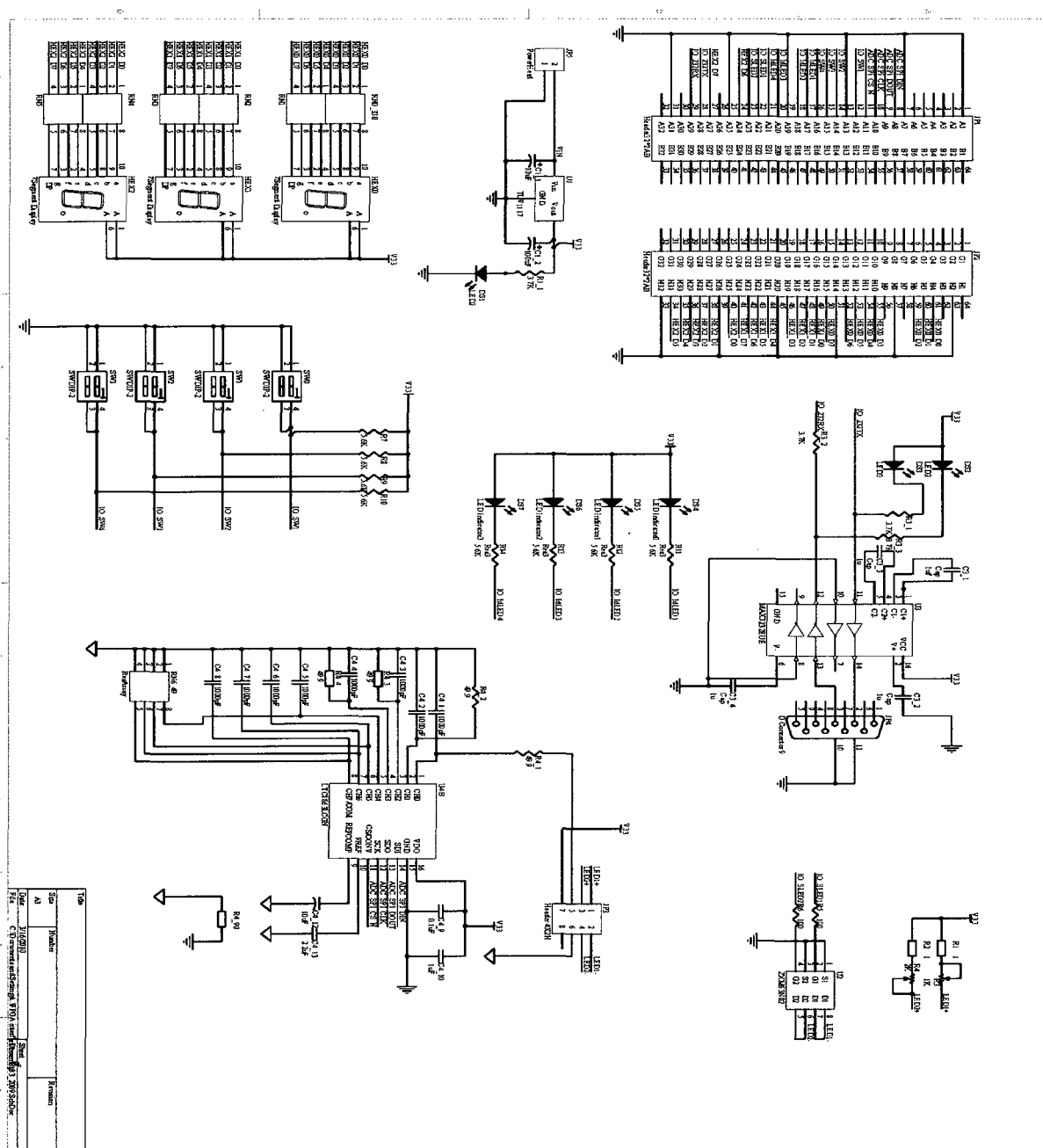


Figure A.1. Schematic of interface circuit board

Table A.1. Pin assignment of the system

Node name	Direction	Location	Function
clk	Input	PIN_E2	System clock
in1_n	Input	PIN_R7	Switch 0
in2_n	Input	PIN_N8	Switch 2
reset_n	Input	PIN_R10	Reset
SDI	Input	PIN_P6	Serial data from the ADC
Srv_Pod_I	Input	PIN_T15	UART RS 232 receiving
befdecsegment[0]	Output	PIN_C16	The first 7-Segment Display, a
befdecsegment[1]	Output	PIN_D16	The first 7-Segment Display, b
befdecsegment[2]	Output	PIN_D15	The first 7-Segment Display, c
befdecsegment[3]	Output	PIN_F15	The first 7-Segment Display, d
befdecsegment[4]	Output	PIN_J13	The first 7-Segment Display, e
befdecsegment[5]	Output	PIN_J16	The first 7-Segment Display, f
befdecsegment[6]	Output	PIN_P16	The first 7-Segment Display, g
befdecsegment[7]	Output	PIN_N12	The first 7-Segment Display, h
cs_conv1	Output	PIN_R6	Signal to initiate conversions on the ADC
dec1segment[0]	Output	PIN_D9	The second 7-Segment Display, a
dec1segment[1]	Output	PIN_E10	The second 7-Segment Display, b
dec1segment[2]	Output	PIN_A10	The second 7-Segment Display, c
dec1segment[3]	Output	PIN_B11	The second 7-Segment Display, d
dec1segment[4]	Output	PIN_F16	The second 7-Segment Display, e

dec1segment[5]	Output	PIN_C15	The second 7-Segment Display, f
dec1segment[6]	Output	PIN_B16	The second 7-Segment Display, g
dec1segment[7]	Output	PIN_F14	The second 7-Segment Display, h
dec2segment[0]	Output	PIN_A2	The third 7-Segment Display, a
dec2segment[1]	Output	PIN_D6	The third 7-Segment Display, b
dec2segment[2]	Output	PIN_C6	The third 7-Segment Display, c
dec2segment[3]	Output	PIN_B5	The third 7-Segment Display, d
dec2segment[4]	Output	PIN_A5	The third 7-Segment Display, e
dec2segment[5]	Output	PIN_D8	The third 7-Segment Display, f
dec2segment[6]	Output	PIN_B7	The third 7-Segment Display, g
dec2segment[7]	Output	PIN_F9	The third 7-Segment Display, h
led1_reslt_indict	Output	PIN_N11	Indicator LED of measurement result
led1_sensr	Output	PIN_R16	Driver signal for LED1 in the sensor
led2_sensr	Output	PIN_L15	Driver signal for LED2 in the sensor
led_restart_indict	Output	PIN_L14	Acknowledgment signal to indicator LED (DS7)
S1_n	Output	PIN_R11	Acknowledgment signal to LED (DS5)
S2_n	Output	PIN_L13	Acknowledgment signal to LED (DS6)
sck1	Output	PIN_R5	Shift clock, which synchronizes the serial data transfer between ADC and FPGA board

SDO	Output	PIN_R4	Transfer configuration word from FPGA board to ADC
Stx_Pod_O	Output	PIN_T13	UART RS 232 sending pod
Uart_Led_Indic	Output	PIN_R6	Indicator of work status of wireless data communication

REFERENCES

- [1]. Powner E.T., Yalcinkaya F. 1997. Intelligent Biosensor, *Sensor Review*, Vol.17, No.2, pp.107-116.
- [2]. Pohanka M, Jun D, Kuca K. 2007. Mycotoxin assay using biosensor technology: a review. *Drug Chem. Toxicol.* 30(3):253-61.
- [3]. Clark HA, Kopelman R, Tjalkens R and Philbert MA. Optical nanosensors for chemical analysis inside single living cells. 2. Sensors for pH and calcium and the intracellular application of PEBBLE sensors. *Anal Chem.* 1999 Nov 1;71(21):4837-43.
- [4]. May C. Morris. 2010. Fluorescent Biosensors of Intracellular Targets from Genetically Encoded Reporters to Modular Polypeptide Probes. *Cell Biochemistry and Biophysics* 56(1):19-37.
- [5]. Mykhailo D. Bilokin', Volodymyr V. Shvadchak and Vasyl G. Pivovarenko. 2009. Dual-Fluorescence Probe of Environment Basicity (Hydrogen Bond Accepting Ability) Displaying no Sensitivity to Polarity. *Journal of Fluorescence* 19(3):545-553.
- [6]. Guenter Gauglitz. 2005. Direct optical sensors: principles and selected applications. *Analytical and Bioanalytical Chemistry*, papers 381,1618-2642.
- [7]. D. Ivnitski, T. Wolf, B. Solomon, G. Fleminger and J. Rishpon. 1998. An amperometric biosensor for real-time analysis of molecular recognition. *Bioelectrochem. Bioenerg.* 45, no. 1, pp. 27-35.
- [8]. R. Ince and R. Narayanaswamy. 2006. Analysis of the performance of interferometry, surface plasmon resonance and luminescence as biosensors and chemosensors review. *Anal. Chim. Acta* 569, no. 1-2, pp. 1-20.
- [9]. J. Homola, S. Yee and G. Gauglitz. 1999. Surface plasmon resonance sensors: review. *Sens. Actuators, B* 54, no. 1-2, pp. 3-15.
- [10]. B. J. Luff, J. S. Wilkinson, J. Piehler, U. Hollenbach, J. Ingenhoff and N. Fabricius. 1998. Integrated optical Mach-Zehnder biosensor. *J. Lightwave Technol.* 16, no. 4, pp. 583-592.
- [11]. F. Prieto, B. Sepúlveda, A. Calle, A. Llobera, C. Domínguez, A. Abad, A. Montoya and L. M. Lechuga. 2003. An integrated optical interferometric nanodevice based on silicon technology for biosensor applications. *J. Nanotechnol.* 14, pp. 907-912.
- [12]. F. Prieto, B. Sepúlveda, A. Calle, A. Llobera, C. Domínguez and L. M. Lechuga. 2003. Integrated Mach-Zehnder interferometer based on ARROW structures for biosensor applications. *Sens. Actuators, B* 92, pp. 151-158.

- [13]. G. H. Cross, A. A. Reeves, S. Brand, J. F. Popplewell, L. L. Peel, M. J. Swann and N. J. Freeman. 2003. A new quantitative optical biosensor for protein characterization. *Biosens. Bioelectron.* 19, no. 4, pp. 383-390.
- [14]. C. A. Barrios, M. J. Bañuls, V. González-Pedro, K. B. Gylfason, B. Sánchez, A. Griol, A. Maquieira, H. Sohlström, M. Holgado and R. Casquel. 2008. Label-free optical biosensing with slot-waveguides. *Opt. Lett.* 33, no. 7, pp. 708-710.
- [15]. A. Ksendzov and Y. Lin. 2005. Integrated optics ring-resonator sensors for protein detection. *Opt. Lett.* 30, no. 24, pp. 3344-3346.
- [16]. J. Vörös, J. J. Ramsden, G. Csúcs, I. Szendrő, S. M. De Paul, M. Textor and N. D. Spencer. 2002. Optical grating coupler biosensors. *Biomaterials* 23, no. 17, pp. 3699-3710.
- [17]. M. Wiki and R. E. Kunz. 2000. Wavelength-interrogated optical sensor for biomedical applications. *Opt. Lett.* 25, no. 7, pp. 463-465.
- [18]. E. Chow, A. Grot, L. W. M. Mirkarimi, M. Sigalas and G. Girolami. 2004. Ultracompact biochemical sensor built with two dimensional photonic crystal microcavity. *Opt. Lett.* 29, no. 10, pp. 1093-1095.
- [19]. P. Domachuck, H. Nguyen, H. C. Eggleton, B. J. Straub and M. Gu. 2004. Microfluidic tunable photonic band-gap device, *Appl. Phys. Lett.* 84, pp. 1838-1840.
- [20]. Wu N, Wang W, Ling Y, Farris LR, Kim B, McDonald MJ and Wang X. 2010. Label-free detection of biomolecules using LED technology. *Proc. SPIE Photonics West BiOS Exhibition* 23–24.
- [21]. B. Sepúlveda, J. Sánchez del Río, M. Moreno, F. J. Blanco, K. Mayora, C. Domínguez and L. M. Lechuga. 2006. Optical biosensor microsystems based on the integration of highly sensitive Mach–Zehnder interferometer devices. *J. Opt. A: Pure Appl. Opt.* 8, pp. S561-S566.
- [22]. Farris, L.R., W. Wang, A.C. Lisa-Jo, X. Wang, and M.J. McDonald. 2009. Influenza a nucleoprotein detection by a novel immuno-interferometric sensor. *Biophysical Journal*, papers 96, 634a-635a.
- [23]. Farris, L.R., N. Wu, W. Wang, A.C. Lisa-Jo, X. Wang and M.J. McDonald. 2009. Immuno-interferometric sensor for the detection of Influenza A Nucleoprotein. *Analytical and Bioanalytical Chemistry, Papers*.
- [24]. Wu N, Wang W, Farris LR, McDonald MJ and Wang X. 2009. Label free detection of biomolecules using an optical biosensor. *Asian-Pacific Network of Centers for Research in Smart Structure Technology*.
- [25]. Wang W, Ma X, Clarizia LJ, Wang X and McDonald MJ. 2009. Optical interferometric biosensor with PMMA as functional layer. *Proc. Mater Res Soc Symp*

- [26]. M. Holgado, R. Casquel, C. Molpeceres, M. Morales and J. L. Ocaña. 2008. Simultaneous reflectivity, ellipsometry and spectrometry measurements in submicron structures for liquid sensing. *Sens. Lett.* 6, no. 4, pp. 564-569.
- [27]. M. Holgado, R. Casquel, B. Sánchez, C. Molpeceres, M. Morales and J. L. Ocaña. 2007. Optical characterization of extremely small volumes of liquid in sub-micro-holes by simultaneous reflectivity, ellipsometry and spectrometry. *Opt. Express* 15, no. 20, pp. 13318-13329.
- [28]. M. Holgado, R. Casquel, María-Fe Laguna, M. Morales, C. Molpeceres and J. L. Ocaña. 2008. Sub-micro holes sensing cells analyzed by Fourier transform IR-visible spectrometry for biochemical sensing. *Proc. Eurosensors*, pp. 668-671.
- [29]. R. Casquel, M. Holgado, A. Lavín, C. A. Barrios, C. Molpeceres, M. Morales, J. L. Ocaña. 2008. Vertical resonant microcavities based on pillars analyzed by beam profile ellipsometry and reflectometry. *Proc. Eurosensors*, pp. 1577-1580.
- [30]. M. Holgado and R. Casquel. 2009. Micro-nano photonic biosensors scalable at the wafer level, *Proc. SPIE*, 2009. Paper accepted at OPTO: Integrated Optoelectronic Devices, SPIE Photonics West in San Jose, California, January 24-29.
- [31]. Grenville Robinson. 1995. The commercial development of planar optical biosensors. *Sensors and Actuators B: Chemical*, Volume 29, Issues 1-3, Pages 31-36.
- [32]. G. Gauglitz. 2005. Direct optical sensors: principles and selected applications. *Anal. Bioanal. Chem.* 381, pp. 141-155.
- [33]. Göpel W, Hesse J and Zemel JN. 1992. *Sensors, a comprehensive survey*. Meas. Sci. Technol. vol I-VIII. VCH, Weinheim.
- [34]. Homola J, Yee S and Myszka D. 2002. Optical biosensors present and future. In: Ligler FS, Rowe T, Chris A (eds) Elsevier, Amsterdam, p 207.
- [35]. C. Hänel and G. Gauglitz, 2002. Comparison of reflectometric interference spectroscopy with other instruments for label-free optical detection. *Anal. Bioanal. Chem.* 372, pp. 91-100.
- [36]. Clarizia, L.-J., D. Sok, M. Wei, J. Mead, C. Barry, and M. McDonald. 2009. Antibody orientation enhanced by selective polymer-protein noncovalent interactions. *Analytical and Bioanalytical Chemistry*, papers 393(5), 1531-1538.
- [37]. Fixe, F., M. Dufva, P. Telleman, and C.B.V. Christensen. 2004. One-step immobilization of aminated and thiolated DNA onto poly(methylmethacrylate) (PMMA) substrates. *Lab on a Chip* papers 4, 191-195.
- [38]. Eugene Hecht. 2001. *Optics*. Addison Wesley, San Francisco, pp. 385-438.

- [39]. Michael F. Toneya, C. Mathew Mate and Daryl Pockerb. 2000. Interferometric biosensor based on planar optical waveguide sensor chips for label-free detection of surface bound bioreactions. *Journal of Colloid and Interface Science*, papers 225, 2591-2597.
- [40]. Reichl D, Krage R, Krummel C, and Gauglitz G. 2000. Sensing of Volatile Organic Compounds Using a Simplified Reflectometric Interference Spectroscopy Setup. *Applied Spectroscopy*, papers 54, 583-586.
- [41]. C. A. Foord, L. D. Wedeven, F. J. Westlake, and A. Cameron. 1967-70. Optical elastohydrodynamics. *Proc. Inst. Mech. Eng.* 184, 487-505 (1969-70).

AUTHOR BIOGRAPHY

Yunfeng Ling was born in China and grew up in Huzhou, Zhejiang province. He received the Bachelor and Master of Engineering Degree from Haerbin Engineering University in the College of Automation at the Department, Haerbin, China, in 2008. He then went to the University of Massachusetts Lowell to pursue a Master of Science Degree in Mechanical Engineering with a specific research focus on nano-technology.

He has obtained two publications during his master's study:

- (1) Ling Y, Wu N, Wang W, Farris LR, Kim B, Wang X, McDonald MJ. 2010. Thin film thickness variation measurement using dual LEDs and reflectometric interference spectroscopy model in biosensor. Proc. SPIE Photonics West BiOS Exhibition 23–24.
- (2) Wu N, Wang W, Ling Y, Farris LR, Kim B, McDonald MJ, Wang X. 2010. Label-free detection of biomolecules using LED technology. Proc. SPIE Photonics West BiOS Exhibition 23–24.